[9] P. Svoboda, P. Stein, H. Hayashi, R.M. Schultz, Selective reduction of dormant maternal mRNAs in mouse oocytes by RNA interference, Development 127 (2000) 4147–4156.
[10] F. Wianny, M. Zernicka-Goetz, Specific interference with gene function by double-stranded RNA in early mouse development, Nat. Cell Biol. 2 (2000) 70–75.
[11] E. Billy, V. Brondani, H. Zhang, U. Muller, W. Filipowicz, Specific interference with gene expression induced by long, double-stranded RNA in mouse embryonal teratocarcinoma cell lines, Proc. Natl. Acad. Sci. USA 98 (2001) 14428–14433.
[12] S. Yang, S. Tutton, E. Pierce, K. Yoon, Specific double-stranded RNA interference in undifferentiated mouse embryonic stem cells, Mol. Cell. Biol. 21 (2001) 7807–7816.
[13] M.R. Player, P.F. Torrence, The 2-5A system: modulation of viral and cellular processes through acceleration of RNA degradation, Pharmacol. Ther. 78 (1998) 55–113.
[14] M. Gale Jr., M.G. Katze, Molecular mechanisms of interferon resistance mediated by viral-directed inhibition of PKR, the interferon-induced protein kinase, Pharmacol. Ther. 78 (1998) 29–46.
[15] S.M. Elbashir, J. Harborth, W. Lendeckel, A. Yalcin, K. Weber, T. Tuschl, Duplexes of 21-nucleotide RNAs mediate RNA interference in cultured mammalian cells, Nature 411 (2001) 494–498.
[16] S. Matsuda, Y. Ichigotani, T. Okuda, T. Irimura, S. Nakatsugawa, M. Hamaguchi, Molecular cloning and characterization of a novel human gene (HERNA) which encodes a putative RNA-helicase, Biochim. Biophys. Acta 1490 (2000) 163–169.
[17] R.H. Nicholson, A.W. Nicholson, Molecular characterization of a mouse cDNA encoding Dicer, a ribonuclease III ortholog involved in RNA interference, Mamm. Genome 13 (2002) 67–73.
[18] P. Provost, D. Dishart, J. Doucet, D. Frendewey, B. Samuelsson, O. Radmark, Ribonuclease activity and RNA binding of recombinant human Dicer, EMBO J. 21 (2002) 5864–5874.
[19] H. Zhang, F.A. Kolb, V. Brondani, E. Billy, W. Filipowicz, Human Dicer preferentially cleaves dsRNAs at their termini without a requirement for ATP, EMBO J. 21 (2002) 5875–5885.
[20] K.S. Yan, S. Yan, A. Farooq, A. Han, L. Zeng, M.M. Zhou, Structure and conserved RNA binding of the PAZ domain, Nature 426 (2003) 468–474.
[21] J. Martinez, A. Patkaniowska, H. Urlaub, R. Luhrmann, T. Tuschl, Single-stranded antisense siRNAs guide target RNA cleavage in RNAi, Cell 110 (2002) 563–574.
[22] N. Doi, S. Zenno, R. Ueda, H. Ohki-Hamazaki, K. Ui-Tei, K. Saigo, Short-interfering-RNA-mediated gene silencing in mammalian cells requires Dicer and eIF2C translation initiation factors, Curr. Biol. 13 (2003) 41–46.
[23] J.D. Rosenblatt, A.I. Lunt, D.J. Parry, T.A. Partridge, Culturing satellite cells from living single muscle fiber explants, In Vitro Cell. Dev. Biol. Anim. 31 (1995) 773–779.
[24] D. Yaffe, O. Saxel, Serial passaging and differentiation of myogenic cells isolated from dystrophic mouse muscle, Nature 270 (1977) 725–727.
[25] H. Hohjoh, RNA interference (RNAi) induction with various types of synthetic oligonucleotide duplexes in cultured human cells, FEBS Lett. 521 (2002) 195–199.
[26] S.M. Hammond, S. Boettcher, A.A. Caudy, R. Kobayashi, G.J. Hannon, Argonaute2, a link between genetic and biochemical analyses of RNAi, Science 293 (2001) 1146–1150.
[27] R.W. Williams, G.M. Rubin, ARGONAUTE1 is required for efficient RNA interference in *Drosophila* embryos, Proc. Natl. Acad. Sci. USA 99 (2002) 6889–6894.
[28] T. Holen, M. Amarzguioui, M.T. Wiiger, E. Babaie, H. Prydz, Positional effects of short interfering RNAs targeting the human coagulation trigger tissue factor, Nucleic Acids Res. 30 (2002) 1757–1766.
[29] K. Omi, K. Tokunaga, H. Hohjoh, Long-lasting RNAi activity in mammalian neurons, FEBS Lett. 558 (2004) 89–95.

Available online at www.sciencedirect.com
SCIENCE DIRECT®
ELSEVIER
Biochemical and Biophysical Research Communications 329 (2005) 516–521
BBRC
www.elsevier.com/locate/ybbrc

Influence of assembly of siRNA elements into RNA-induced silencing complex by fork-siRNA duplex carrying nucleotide mismatches at the 3′- or 5′-end of the sense-stranded siRNA element

Yusuke Ohnishi [a,b], Katsushi Tokunaga [b], Hirohiko Hohjoh [a,*]

[a] *National Institute of Neuroscience, NCNP, 4-1-1 Ogawahigashi, Kodaira, Tokyo 187-8502, Japan*
[b] *Department of Human Genetics, Graduate School of Medicine, The University of Tokyo, 7-3-1 Hongo, Bunkyo-ku, Tokyo 113-0033, Japan*

Received 27 January 2005

Abstract

RNA interference (RNAi) is a powerful method for suppressing the expression of a gene of interest, and can be induced by 21–25 nucleotide small interfering RNA (siRNA) duplexes homologous to the silenced gene, which function as sequence-specific RNAi mediators in RNA-induced silencing complexes (RISCs). In the previous study, it was shown that fork-siRNA duplexes, whose sense-stranded siRNA elements carried a few nucleotide mismatches at the 3′-ends against the antisense-stranded siRNA elements, could enhance RNAi activity more than conventional siRNA duplexes in cultured mammalian cells. In this study, we further characterized fork-siRNA duplexes using reporter plasmids carrying target sequences complementary to the sense- or antisense-stranded siRNA elements in the untranslated region of *Renilla* luciferase. The data presented here suggest that nucleotide mismatches at either the 3′- or 5′-end of the sense-stranded siRNA elements in fork-siRNA duplexes could influence assembly of not only the antisense-stranded siRNA elements but also the sense-stranded elements into RISCs. In addition, we further suggest the possibility that there could be a positional effect of siRNA duplex on RNAi activity.

Keywords: RNA interference; Fork-siRNA; Mismatch; RNAi mediator; RISC

RNA interference (RNAi) is the process of a sequence-specific post-transcriptional gene silencing triggered by double-stranded RNAs (dsRNAs) homologous to the silenced gene (reviewed in [1–4]). DsRNAs introduced or generated in cells are subjected to digestion with an RNase III enzyme, Dicer, into 21–25 nucleotide (nt) RNA duplexes [5–8], and the resultant RNA duplexes, referred to as small interfering RNA (siRNA) duplexes, can be associated with the RNA-induced silencing complexes (RISCs) and function as sequence-specific RNAi mediators in the complexes [5,7]. In terms of rapid and potent induction of RNAi by exogenous dsRNAs, RNAi has become a powerful reverse genetic tool for suppressing the expression of a gene of interest in various species including mammals.

In mammals, direct introduction of chemically synthesized 21–25 nt siRNA duplexes into cells is often used for induction of RNAi [9–12], although different siRNAs induce different levels of RNAi activities [10,13]. In previous studies, where the effect of various types of synthetic siRNAs on the induction of mammalian RNAi was tested, an improvement of the siRNA duplexes for enhancing RNAi activity was found [14]. The improved siRNA duplexes, named 'fork-siRNA duplexes,' possess mismatched sequences at their termini due to introduction of base substitutions into the

* Corresponding author. Fax: +81 42 346 1748.
E-mail address: hohjohh@ncnp.go.jp (H. Hohjoh).

0006-291X/$ - see front matter © 2005 Elsevier Inc. All rights reserved.
doi:10.1016/j.bbrc.2005.02.012

3′-ends of the sense-stranded siRNA elements: one of the ends of the fork-siRNA duplex, on the 3′-end of the sense-stranded siRNA element, remains open (unannealed). In addition to the properties of fork-siRNA duplex, recent studies suggested that siRNA duplexes conferring a strong RNAi activity could be characterized by a low base-stability due to AU-rich sequences around the 3′-ends of the sense-stranded siRNA elements, i.e., the functional siRNA duplexes have the asymmetrical features of the AU (or GC) content in their sequences [14–16]. Based on these observations, a model was proposed: the ease of unwinding from one of the ends of the siRNA duplex could determine the orientation of the duplex, and the siRNA element unwound from the 5′-end could be determined and function as a sequence-specific RNAi mediator in RISC [14].

In order to further characterize fork-siRNA duplexes, we report herein the construction of reporter plasmids carrying target sequences complementary to the sense- and antisense-stranded siRNA elements, and examination of the levels of gene silencing depending upon the sense- and antisense-stranded siRNA elements functioning as RNAi mediators in RISCs. The data presented here suggested that the structural features of fork-siRNA duplexes could influence incorporation of their siRNA elements into RISCs.

Materials and methods

Preparation of oligonucleotides. RNA and DNA synthetic oligonucleotides were obtained from PROLIGO and INVITROGEN, respectively. For preparation of duplexes, sense- and antisense-stranded oligonucleotides (20 μM each) were mixed in an annealing buffer (30 μM Hepes, pH 7.4, 100 μM potassium acetate, and 2 μM magnesium acetate), heat-denatured at 90 °C for 3 min, and annealed at 37 °C overnight. The siRNA duplexes used in this study were as follows: the La21-conv. siRNA duplex (a conventional siRNA duplex), La21-3′m2 siRNA duplex (a fork-siRNA duplex carrying two-base mismatches at the 3′-end of the sense-stranded siRNA element), La21-5′m2 siRNA duplex (a fork-siRNA duplex carrying two-base mismatches at the 5′-end of the sense-stranded siRNA element), and La21-ss19 siRNA duplex (a siRNA duplex containing 19 nt sense-stranded siRNA element) (Fig. 1B) [14]. Note that these La21 siRNA duplexes possess the same antisense-stranded siRNA elements. Non-silencing siRNA duplex (Qiagen) was used as a negative control.

Construction of reporter plasmids. In order to insert target sequence complementary to the sense- or antisense-stranded La21 siRNA element [10] against *Photinus* luciferase in the 3′ untranslated region (UTR) of the *Renilla* luciferase transcripts, the phRL-TK plasmid (Promega) carrying the *Renilla* luciferase gene was digested with *Xba*I and *Not*I, and subjected to ligation with synthetic oligonucleotide duplexes carrying the La21 siRNA target sequences. The sequences of the synthesized oligonucleotides were as follows:

sLa21Fw; 5′-CTAGCATGCAACCGCTGGAGAGCAACTGCA-3′
asLa21Fw; 5′-GGCCTGCAGTTGCTCTCCAGCGGTTGCATG-3′
sLa21Rv; 5′-CTAGCATGCAGCAGTTGCTCTCCAGCGGTA-3′
asLa21Rv; 5′-GGCCTACCGCTGGAGAGCAACTGCTGCATG-3′

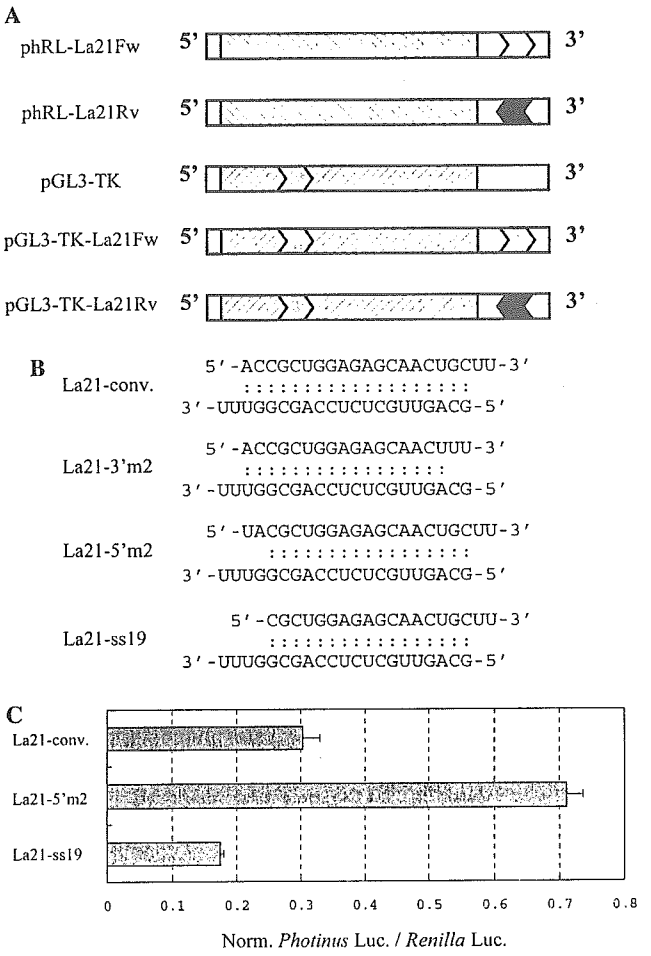

Fig. 1. Schematic drawing of the luciferase transcripts derived from plasmids constructed in this study (A), used synthetic siRNA duplexes (B), and RNAi activities induced by the siRNA duplexes (C). (A) The names of constructed plasmids are indicated. Hatched and open boxes represent the luciferase coding and untranslated regions, respectively. Gray and solid (black) regions indicate target sequences complementary to the antisense- and sense-stranded La21 siRNA elements, respectively. (B) The names of synthetic La21 siRNA duplexes are indicated. Upper and lower sequences in the duplexes represent the sense- and antisense-stranded siRNA elements, respectively. (C) Gene silencing of the *Photinus* luciferase gene. RNAi induction was carried out as described previously [14]. Indicated La21 siRNA duplexes together with pGL3-control and phRL-TK plasmids carrying *Photinus* and *Renilla* luciferase genes, respectively, were transfected into HeLa cells. Twenty-four hours after transfection, cell lysate was prepared and the level of luciferase activity was examined. Ratios of normalized target (*Photinus*) luciferase activity to control (*Renilla*) luciferase activity are shown: the ratios of luciferase activity determined in the presence of the La21 siRNA duplexes were normalized to the ratio obtained for a control in the presence of a non-silencing siRNA duplex (Qiagen). Data are averages of at least three independent determinations. Error bars represent standard deviations.

The resultant plasmids possessing the target sequences for the antisense- and sense-stranded La21 siRNA elements were named 'phRL-La21Fw' and 'phRL-La21Rv,' respectively.

We further constructed reporter plasmids carrying two target sites of the La21 siRNA duplex. The *Hin*dIII–*Xba*I fragment encoding the *Photinus* luciferase gene was isolated from the pGL3-control plasmid

(Promega), and substituted for the *Hin*dIII–*Xba*I regions carrying *Renilla* luciferase in the phRL-La21Fw and phRL-La21Rv plasmids. The resultant plasmids derived from the phRL-La21Fw and phRL-La21Rv plasmids were named 'pGL3-TK-La21Fw' and 'pGL3-TK-La21Rv,' respectively, and possessed two La21 siRNA duplex target sites, one in the *Photinus* luciferase coding region and the other in the 3′ UTR. We also constructed 'pGL3-TK' plasmid by substitution of *Photinus* luciferase for *Renilla* luciferase in the phRL-TK plasmid using the same procedure described above.

Cell culture, transfection, and luciferase and β-galactosidase assays. HeLa cells were grown as described previously [10]. The day before transfection, cells were trypsinized, diluted with fresh medium without antibiotics, and seeded into 24-well culture plates (approximately 0.5×10^5 cells/well). Cotransfection of synthetic siRNA duplexes with reporter plasmids was carried out using Lipofectamine 2000 transfection reagent (Invitrogen) according to the manufacturer's instructions, and to each well, 0.24 μg siRNA duplexes, 0.05 μg phRL-La21Fw or phRL-La21Rv plasmid, and 0.1 μg pSV-β-galactosidase control vector (Promega) as a control were applied. Twenty-four hours after transfection, cell lysate was prepared and the expression levels of luciferase and β-galactosidase were examined by a Dual-Luciferase reporter assay system (Promega) and a Beta-Glo assay system (Promega), respectively, according to the manufacturer's instructions. In the case of transfection with pGL3-TK, pGL3-Tk-La21Fw or pGL3-TK-La21Rv, 0.24 μg siRNA duplexes, 0.1 μg of any one of the pGL3-TK, pGL3-Tk-La21Fw, and pGL3-TK-La21Rv plasmids, and 0.05 μg of the phRL-TK plasmid as a control were applied into HeLa cells. Twenty-four hours after transfection, a Dual-Luciferase reporter assay was conducted.

Results and discussion

Influence of assembly of siRNA elements into RISCs by fork-siRNA duplexes

In the previous study, it was shown that fork-siRNA duplexes carrying nucleotide mismatches at the 3′-ends of the sense-stranded siRNA elements could enhance RNAi activity more than conventional siRNA duplexes [14]. This suggests the possibility of greater occurrence of assembly of the antisense-stranded siRNA elements rather than the sense-stranded elements into RISCs in fork-siRNA duplexes over that in conventional duplexes. Accordingly, we attempted to examine whether fork-siRNA duplexes could influence incorporation of their siRNA elements into RISCs. To address this, we constructed two reporter plasmids, phRL-La21Rv and phRL-La21Fw, carrying the target sequences for the sense- and antisense-stranded La21 siRNA elements, respectively, in the 3′ untranslated region (UTR) of *Renilla* luciferase (Fig. 1A). This is because the previous study showed that the La21-conv., La21-3′m2, and La21-5′m2 siRNA duplexes (Fig. 1B) could confer different levels of RNAi activities, although they possessed the same antisense-stranded siRNA element [14]. In addition to the previous results, the result with a newly designed siRNA duplex, the La21-ss19 siRNA duplex (Figs. 1B and C), also supported the idea that the forked terminus of siRNA duplex could influence RNAi activity. Accordingly, we decided to use the sequences of the sense- and antisense-stranded La21 siRNA elements as targets in this study. Using the phRL-La21Fw and -La21Rv plasmids, and a series of the La21 siRNA duplexes, the levels of gene silencing depending upon the sense- and antisense-stranded La21 siRNA elements were investigated.

First we examined if the sense-stranded siRNA elements, like the antisense-stranded siRNA elements, could have potential for functioning as sequence-specific RNAi mediators in RISCs. To see this, the La21-conv. siRNA duplex together with phRL-La21Rv, phRL-La21Fw or phRL-TK and pSV-β-galactosidase control vector as a control were cotransfected into HeLa cells, and the levels of the expression of *Renilla* luciferase were examined. As a result, significant suppression of the expression of *Renilla* luciferase was detectable in the presence of either phRL-La21Rv or phRL-La21Fw, whereas little or no suppression was seen in the presence of phRL-TK as a negative control (Fig. 2). Therefore, these results strongly suggest that either the sense- or antisense-stranded La21 siRNA element can be incorporated into RISC and function as a sequence-specific RNAi mediator in the complex.

We next examined the RNAi activities directed by the sense- and antisense-stranded siRNA elements derived from the La21-3′m2 and La21-5′m2 siRNA duplexes (fork-siRNA duplexes) as well as the La21-conv. siRNA duplex. As shown in Fig. 3A, when the phRL-La21Fw plasmid was used, ~86%, 95%, and 72% gene silencing mediated by the antisense-stranded La21 siRNA elements derived from the La21-conv., La21-3′m2, and

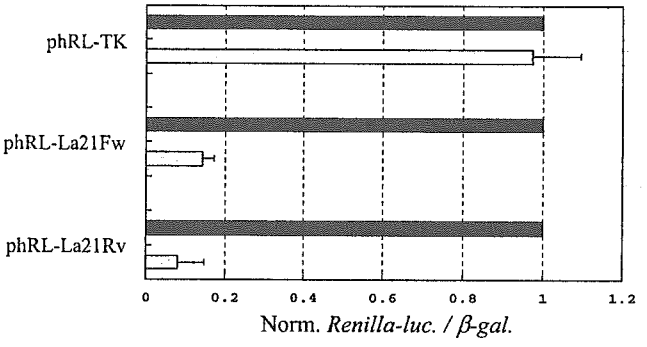

Fig. 2. Gene silencing of exogenous reporter gene with conventional siRNA duplexes. The conventional La21 (La21-conv.) siRNA duplex against the *Photinus* luciferase gene together with phRL-TK, phRL-La21Fw, or phRL-La21Rv plasmid carrying the *Renilla* luciferase reporter gene, and pSV-β-galactosidase control vector as a control were cotransfected into HeLa cells. Twenty-four hours after transfection, cell lysate was prepared, and the levels of the luciferase and β-galactosidase activities were examined. Ratios of normalized target (*Renilla*) luciferase activity to control β-galactosidase activity are shown: the ratios of luciferase activity determined in the presence of the La21-conv. siRNA duplex (gray bars) are normalized to the ratio obtained for a control in the presence of a non-silencing siRNA duplex (Qiagen) (solid bars). Data are averages of at least four independent experiments. Error bars represent standard deviations.

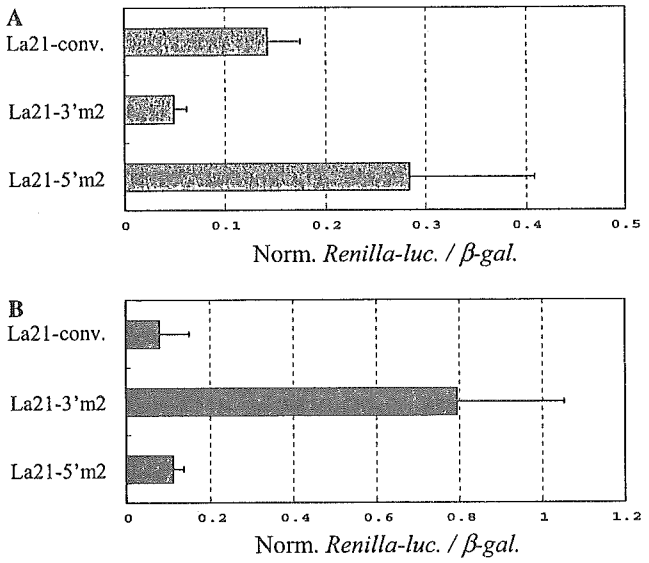

Fig. 3. Silencing of the expression of exogenous reporter gene with various types of siRNA duplexes. The conventional La21 (La21-conv.) or fork-La21 (La21-3′m2 and La21-5′m2) siRNA duplexes together with phRL-La21Fw (A) or phRL-La21Rv (B) reporter plasmid and pSV-β-galactosidase control vector as a control were cotransfected into HeLa cells, and the expression levels of luciferase and β-galactosidase were examined as in Fig. 2. Ratios of normalized target (*Renilla*) luciferase activity to control β-galactosidase activity are shown as in Fig. 2. Data are averages of at least four independent determinations. Error bars indicate standard deviations.

La21-5′m2 siRNA duplexes, respectively, was observed. Although the levels of the gene silencing with phRL-La21Fw as a reporter plasmid increased further than those with the pGL3-control plasmid carrying *Photinus* luciferase in the previous study [14] (further discussion below), the effects of mismatches at the 3′- and 5′-ends of the sense-stranded elements in the La21 fork-siRNA duplexes on RNAi activity appeared to remain unchanged in the experiments using either phRL-La21Fw or pGL3-control.

When the phRL-La21Rv plasmid was used, i.e., when the levels of the RNAi activity directed by the sense-stranded La21 siRNA elements were examined, significant differences in the level of RNAi activity among the La21 siRNA duplexes used were observed: while ~92% and 89% suppression of the expression of *Renilla* luciferase was detectable in the presence of the La21-conv., and La21-5′m2 siRNA duplexes, respectively, the gene silencing mediated by the sense-stranded element derived from the La21-3′m2 duplex appeared to confer ~20% inhibition of the expression of *Renilla* luciferase (Fig. 3B), suggesting that the degree of assembly of the sense-stranded siRNA element into RISC in the La21-3′m2 siRNA duplex could be much lower than those in the La21-conv., and La21-5′m2 siRNA duplexes. Taking all the data together, these observations suggest that nucleotide mismatches at the ends of fork-siRNA duplexes can influence assembly of not only the antisense-stranded siRNA elements but also the sense-stranded siRNA elements into RISCs.

The previous in vitro RNAi reaction with *Drosophila* embryo lysate has demonstrated that single nucleotide mismatch around the termini of siRNA duplex can affect target-RNA cleavages directed by the sense- and antisense-stranded siRNA elements [15]. The results of our present study using cultured human cells consistently agree with those in the previous study. Therefore, it appears that the effect of low base-pairing stabilities due to either AU-rich or nucleotide mismatches around the termini of siRNA duplexes on RNAi activity is likely common among various species. In addition, such low base-pairing stability could contribute to ready unwinding of the duplex from that end by a possible helicase activity in RISCs.

Another important point to note in this study is that the sense-stranded siRNA elements have potential for functioning as sequence-specific RNAi mediators in RISCs. As previously suggested [14], this indicates that off-target gene silencing mediated by the sense-stranded siRNA elements could occur in RNAi induction by siRNA duplexes. Our present data also indicated a possible avoidance of such off-target gene silencing: fork-siRNA duplexes carrying nucleotide mismatches at the 3′-end of the sense-stranded elements could reduce such off-target silencing. Therefore, fork-siRNA duplexes may provide us with not only an increase in RNAi activity but also decrease in off-target gene silencing directed by the sense-stranded siRNA elements.

Positional effect of siRNA target site on RNAi activity

The results shown in Fig. 3A led us to the possibility that the position of an siRNA target site on a silenced gene transcript could influence its RNAi activity, i.e., there could be a positional effect of the siRNA target site on RNAi activity. To examine this possibility, we constructed two reporter plasmids carrying *Photinus* luciferase, pGL3-TK-La21Rv and pGL3-TK-La21Fw, whose 3′ UTRs contained the target sequences complementary to the sense- and antisense-stranded La21 siRNA elements, respectively (Fig. 1A). Thus, the resultant *Photinus* luciferase transcripts derived from pGL3-TK-La21Fw and pGL3-TK-La21Rv possess two target sites: one site complementary to the antisense-stranded La21 siRNA element is in the luciferase coding region, and the other complementary to the sense- or antisense-stranded siRNA element is in its 3′ UTR.

The La21-conv., La21-3′m2, or La21-5′m2 siRNA duplexes together with the pGL3-TK (carrying one target site in the luciferase coding region), pGL3-TK-La21Rv or pGL3-TK-La21Fw plasmid (Fig. 1A) and the phRL-TK plasmid as a control were cotransfected into HeLa cells, and the levels of RNAi activity were examined by a dual-luciferase assay. When the

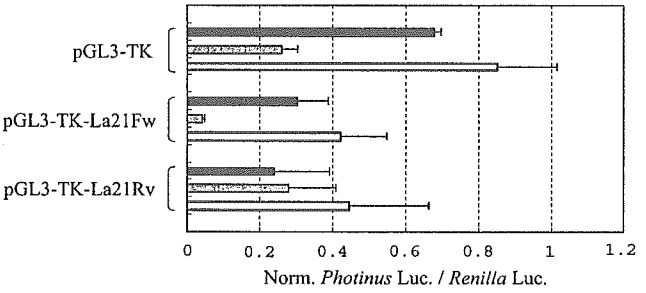

Fig. 4. Gene silencing of *Photinus* luciferase carrying two target sites of the La21 siRNA duplex. The La21-conv., La21-3′m2 or La21-5′m2 siRNA duplex together with pGL3-TK, pGL3-TK-La21Fw or pGL3-TK-La21Rv reporter plasmid carrying *Photinus* luciferase and phRL-TK plasmid carrying *Renilla* luciferase as a control were cotransfected into HeLa cells, and the expression levels of luciferase were examined as in Fig. 1. Ratios of normalized target (*Photinus*) luciferase activity to control (*Renilla*) luciferase activity are shown as in Fig. 1. Solid, gray, and open bars indicate the data in the presence of the La21-conv., La21-3′m2, and La215′m2 siRNA duplexes, respectively. Data are averages of at least three independent determinations. Error bars represent standard deviations.

pGL3-TK plasmid was used, results similar to those in the previous study using the pGL3-control plasmid encoding *Photinus* luciferase driven by the SV40 promoter [14] were observed (Fig. 4). When the pGL3-TK-La21Fw and pGL3-TK-La21Rv plasmids were used, the levels of RNAi activity, other than those in the presence of the pGL3-TK-La21Rv plasmid and the La21-3′m2 siRNA duplex, appeared to increase more greatly in both the pGL3-TK-La21Fw and pGL3-TK-La21Rv plasmids than in the pGL3-TK plasmid used, suggesting that two target sites of the La21 siRNA duplex on the silenced *Photinus* luciferase transcript probably contributed to the enhancement of RNAi activity. As for the RNAi activity in the presence of pGL3-TK-La21Rv and the La21-3′m2 siRNA duplex, it may be that the target site in the luciferase coding region, not in the 3′ UTR, is only recognizable for active RISCs, since a rather weak RNAi activity mediated by the sense-stranded siRNA element in the La21-3′m2 siRNA duplex was detected in the presence of phRL-La21Rv (Fig. 3B). This may account for the lack of significant difference in the level of RNAi activity between pGL3-TK and pGL3-TK-La21Rv in the presence of the La21-3′m2 siRNA duplex.

It should be noted that the La21-5′m2 siRNA duplex was able to confer ~60% suppression of the expression of *Photinus* luciferase in pGL3-TK-La21Fw, although the duplex was able to induce ~15% inhibition of the *Photinus* luciferase expression in pGL3-TK. Since the *Photinus* luciferase transcripts derived from pGL3-TK-La21Fw carry two identical target sites complementary to the antisense-stranded La21 siRNA element, and since the target site in the luciferase coding region appeared not to contribute much to gene silencing when using the La21-5′m2 siRNA duplex (Fig. 4), it is conceivable that the target site in the 3′ UTR could be more sensitive to cleavage by RISCs than that in the luciferase coding region on the *Photinus* luciferase transcripts derived from pGL3-TK-La21Fw in the presence of the La21-5′m2 siRNA duplex. These observations thus suggest a possible positional effect of target site of siRNA duplex on RNAi activity.

Finally, we add that a difference in RNAi activity between phRL-La21Rv (Fig. 3) and pGL3-TK-La21Rv in the presence of the La21-5′m2 siRNA duplex was observed, although the *Renilla* and *Photinus* luciferase transcripts derived from phRL-La21Rv and pGL3-TK-La21Rv, respectively, which carried the same target sites complementary to the sense-stranded La21 siRNA element in their 3′ UTRs, could be subjected to gene silencing chiefly mediated by the sense-stranded siRNA element. The difference might be attributable to possibly different stabilities between the *Renilla* and *Photinus* luciferase gene products in cells. To further evaluate such a possible difference and also the positional effect of siRNA target site on RNAi activity, more extensive studies need to be carried out.

Acknowledgments

We thank Dr. K. Kaneko for his encouragement and support. We also thank Y. Tamura and K. Omi for their helpful cooperation. This work was supported in part by research grants from the Ministry of Health, Labor, Welfare in Japan, and by a Grant-in-Aid from the Japan Society for the Promotion of Science.

References

[1] P.A. Sharp, RNAi and double-strand RNA, Genes Dev. 13 (1999) 139–141.
[2] J.M. Bosher, M. Labouesse, RNA interference: genetic wand and genetic watchdog, Nat. Cell. Biol. 2 (2000) E31–E36.
[3] H. Vaucheret, C. Beclin, M. Fagard, Post-transcriptional gene silencing in plants, J. Cell Sci. 114 (2001) 3083–3091.
[4] H. Cerutti, RNA interference: traveling in the cell and gaining functions? Trends Genet. 19 (2003) 39–46.
[5] S.M. Hammond, E. Bernstein, D. Beach, G.J. Hannon, An RNA-directed nuclease mediates post-transcriptional gene silencing in *Drosophila* cells, Nature 404 (2000) 293–296.
[6] P.D. Zamore, T. Tuschl, P.A. Sharp, D.P. Bartel, RNAi: double-stranded RNA directs the ATP-dependent cleavage of mRNA at 21 to 23 nucleotide intervals, Cell 101 (2000) 25–33.
[7] E. Bernstein, A.A. Caudy, S.M. Hammond, G.J. Hannon, Role for a bidentate ribonuclease in the initiation step of RNA interference, Nature 409 (2001) 363–366.
[8] S.M. Elbashir, W. Lendeckel, T. Tuschl, RNA interference is mediated by 21- and 22-nucleotide RNAs, Genes Dev. 15 (2001) 188–200.
[9] S.M. Elbashir, J. Harborth, W. Lendeckel, A. Yalcin, K. Weber, T. Tuschl, Duplexes of 21-nucleotide RNAs mediate RNA

interference in cultured mammalian cells, Nature 411 (2001) 494–498.
[10] H. Hohjoh, RNA interference (RNAi) induction with various types of synthetic oligonucleotide duplexes in cultured human cells, FEBS Lett. 521 (2002) 195–199.
[11] K. Omi, K. Tokunaga, H. Hohjoh, Long-lasting RNAi activity in mammalian neurons, FEBS Lett. 558 (2004) 89–95.
[12] N. Sago, K. Omi, Y. Tamura, H. Kunugi, T. Toyo-oka, K. Tokunaga, H. Hohjoh, RNAi induction and activation in mammalian muscle cells where Dicer and eIF2C translation initiation factors are barely expressed, Biochem. Biophys. Res. Commun. 319 (2004) 50–57.
[13] T. Holen, M. Amarzguioui, M.T. Wiiger, E. Babaie, H. Prydz, Positional effects of short interfering RNAs targeting the human coagulation trigger tissue factor, Nucleic Acids Res. 30 (2002) 1757–1766.
[14] H. Hohjoh, Enhancement of RNAi activity by improved siRNA duplexes, FEBS Lett. 557 (2004) 193–198.
[15] D.S. Schwarz, G. Hutvagner, T. Du, Z. Xu, N. Aronin, P.D. Zamore, Asymmetry in the assembly of the RNAi enzyme complex, Cell 115 (2003) 199–208.
[16] A. Khvorova, A. Reynolds, S.D. Jayasena, Functional siRNAs and miRNAs exhibit strand bias, Cell 115 (2003) 209–216.

BIOLOGY OF REPRODUCTION 73, 29–35 (2005)
Published online before print 2 March 2005.
DOI 10.1095/biolreprod.104.037077

Ubiquitin C-Terminal Hydrolase L-1 Is Essential for the Early Apoptotic Wave of Germinal Cells and for Sperm Quality Control During Spermatogenesis[1]

Jungkee Kwon,[3,4] Keiji Mochida,[5] Yu-Lai Wang,[3] Satoshi Sekiguchi,[4] Tadashi Sankai,[6] Shunsuke Aoki,[3] Atsuo Ogura,[5] Yasuhiro Yoshikawa,[4] and Keiji Wada[2,3]

Department of Degenerative Neurological Disease,[3] National Institute of Neuroscience, National Center of Neurology and Psychiatry, Kodaira, Tokyo 187-8502, Japan
Department of Biomedical Science,[4] Graduate School of Agricultural and Life Sciences, University of Tokyo, Bunkyo-ku, Tokyo 113-8657, Japan
Bioresource Engineering Division,[5] Bioresource Center, Riken, Tsukuba, Ibaraki 305-0074, Japan
Tsukuba Primate Center,[6] National Institute of Infectious Diseases, Tsukuba, Ibaraki 305-0843, Japan

ABSTRACT

Ubiquitination is required throughout all developmental stages of mammalian spermatogenesis. Ubiquitin C-terminal hydrolase (UCH) L1 is thought to associate with monoubiquitin to control ubiquitin levels. Previously, we found that UCHL1-deficient testes of *gad* mice have reduced ubiquitin levels and are resistant to cryptorchid stress-related injury. Here, we analyzed the function of UCHL1 during the first round of spermatogenesis and during sperm maturation, both of which are known to require ubiquitin-mediated proteolysis. Testicular germ cells in the immature testes of *gad* mice were resistant to the early apoptotic wave that occurs during the first round of spermatogenesis. TUNEL staining and cell quantitation demonstrated decreased germ cell apoptosis and increased numbers of premeiotic germ cells in *gad* mice between Postnatal Days 7 and 14. Expression of the apoptotic proteins TRP53, Bax, and caspase-3 was also significantly lower in the immature testes of *gad* mice. In adult *gad* mice, cauda epididymidis weight, sperm number in the epididymis, and sperm motility were reduced. Moreover, the number of defective spermatozoa was significantly increased; however, complete infertility was not detected. These data indicate that UCHL1 is required for normal spermatogenesis and sperm quality control and demonstrate the importance of UCHL1-dependent apoptosis in spermatogonial cell and sperm maturation.

apoptosis, early apoptotic wave, epididymis, gad *mouse, sperm, spermatogenesis, sperm quality, testis, UCHL1*

INTRODUCTION

Ubiquitin and ubiquitin-dependent proteolysis are involved in a variety of cellular processes, such as cell cycle progression, degradation of intracellular proteins, programmed cell death, and membrane receptor endocytosis [1–5]. In spermatogenesis, the ubiquitin-proteasome system is required for the degradation of numerous proteins throughout the mitotic, meiotic, and postmeiotic developmental phases [4, 6, 7]. Ubiquitin C-terminal hydrolases (UCHs) control the cellular ubiquitin balance by releasing ubiquitin from tandemly conjugated ubiquitin monomers (*Ubb, Ubc*) and small adducts or unfolded polypeptides [4, 8–10]. UCHL1 is expressed at high levels in both testis and epididymis and may play an important role in the regulation of spermatogenesis [11–14]. In addition to its hydrolase activity [15], UCHL1 has a variety of functions, including dimerization-dependent ubiquityl ligase activity, and association with and stabilization of monoubiquitin in neuronal cells [16–18]. Furthermore, it has been suggested that UCHL1 also functions as a regulator of apoptosis [19]. The gracile axonal dystrophy (*gad*) mouse is an autosomal recessive spontaneous mutant carrying an intragenic deletion of the gene encoding *Uchl1* [21]. We recently found that testes of *gad* mice, which lack UCHL1 expression [18, 20, 21], have reduced ubiquitin levels and are resistant to cryptorchid injury-mediated germ cell apoptosis [22].

During prepubertal development, an early and massive wave of germinal cell apoptosis occurs in mouse testis [23, 24]. This early germ cell apoptotic wave affects mainly spermatogonia and spermatocytes and appears to be essential for functional spermatogenesis in adulthood. Decreased apoptosis has been reported in the early phase of spermatogenesis in transgenic mice overexpressing the antiapoptotic proteins *Bcl2* or *Bcl-xL* [23, 25] and in mice deficient in the apoptotic protein *Bax* [26]. This reduction in apoptosis is associated with the disruption of normal spermatogenesis and infertility. Our previous work demonstrated that *gad* mice exhibit pathological changes such as progressively decreasing spermatogonial stem cell proliferation [13] and increased expression of the antiapoptotic proteins Bcl2 and Bcl-xL in response to apoptotic stress [19, 22]. Furthermore, we showed that UCHL1 functions during prepubertal development to effect normal spermatogenesis and to modulates germ cell apoptosis [22]. However, the mechanism by which UCHL1 regulates apoptosis during prepubertal development remains unclear. To further investigate the role of UCHL1 in immature testes, we evaluated the function of UCHL1 during early spermatogenesis. Here, we show that immature testes of *gad* mice accumulate premeiotic germ cells and are resistant to the massive wave of germinal cell apoptosis during the first round of spermatogenesis, eventually leading to alterations in sperm produc-

[1]Supported by Grants-in-Aid for Scientific Research from the Ministry of Health, Labour and Welfare of Japan; Grants-in-Aid for Scientific Research from the Ministry of Education, Culture, Sports, Science and Technology of Japan; a grant from the Pharmaceuticals and Medical Devices Agency of Japan; and a grant from Japan Science and Technology Agency.
[2]Correspondence: Keiji Wada, Department of Degenerative Neurological Disease, National Institute of Neuroscience, National Center of Neurology and Psychiatry, Kodaira, Tokyo 187-8502, Japan.
FAX: 81 42 341 1745; e-mail: wada@ncnp.go.jp

Received: 16 October 2004.
First decision: 16 December 2004.
Accepted: 21 February 2005.

ISSN: 0006-3363. http://www.biolreprod.org

tion, motility, and morphology in adult mice. Our data suggest that UCHL1-dependent apoptosis is essential for normal spermatogenesis.

MATERIALS AND METHODS

Animals

We used male *gad* (CBA/RFM) mice [21] at 7, 14, 21, 28, and 35 days and 10 wk of age. The *gad* mouse is an autosomal-recessive mutant that was produced by crossing CBA and RFM mice. The *gad* line was maintained by intercrossing for more than 20 generations. This strain was maintained at our institute. Animal care and handling were in accordance with institutional regulations and were approved by the Animal Investigation Committee of the National Institute of Neuroscience, National Center of Neurology and Psychiatry.

Histological and Immunohistochemical Assessment of Testes

Testes were embedded in paraffin wax after fixation in 4% paraformaldehyde, sectioned at 4-μm thickness, and stained with hematoxylin for counting [13]. Light microscopy was used for routine observations. For immunohistochemical staining, the sections were incubated with 10% goat serum for 1 h at room temperature followed by incubation overnight at 4°C with a rabbit polyclonal antibody against UCHL1 (1:1000 dilution; peptide antibody) [20] in PBS containing 1% BSA. Sections were then incubated for 1 h with biotin-conjugated anti-rabbit IgG diluted 1:200 in PBS, followed by Vectorstain ABC-PO (Vector Laboratories, Burlingame, CA) for 30 min at room temperature. Sections were developed using 3,3′-diaminobenzidine and counterstained with hematoxylin.

Apoptotic cells in testicular tissues were identified by terminal deoxynucleotidyl transferase (TdT)-mediated nick end labeling (TUNEL) using the DeadEnd Fluorometric TUNEL system (Promega, Madison, WI) according to the manufacturer's instructions.

Quantitative Analysis of Testicular Cell Number

The total number of cells was determined by counting the testicular cells including Sertoli cells of seminiferous tubules. Quantitative determinations were made using four each of wild-type and *gad* mice at 7 and 14 days of age. Five sections from each mouse were processed in parallel for counterstaining with hematoxylin. Twenty circular seminiferous tubules in each section were then selected by randomly from those tubules, and 400 circular seminiferous tubules were measured using the 400× lens of a Zeiss Axioplan microscope. The total cell number was not determined by dividing cell types such as testicular germ cells and Sertoli cells because it was difficult to determine the difference of cell types [26]. There were no significant differences in nuclear size in either of the group studies. Thus, the total number of cells reflected all cell types of seminiferous tubules.

Quantitative Analysis of Apoptotic Germ Cells

Quantification was performed using four each of wild-type and *gad* mice at 7, 14, 21, 28, and 35 days of age. The total number of apoptotic cells was determined by counting the positively stained nuclei in 20 circular seminiferous tubules in each section [22]. Five sections from each mouse and a total 400 circular seminiferous tubules per each group were processed.

Germ Cell Isolation, Culture, and Viability Measurement

Germ cells from wild-type and *gad* mice were prepared using a modification of the procedure described by Kwon et al. [20]. Briefly, testes from three 2-wk-old mice were incubated twice for 30 min at 25°C in Dulbecco Modified Eagle medium (DMEM)-F12 medium containing 0.5 mg/ml collagenase IV-S (Sigma-Aldrich, St. Louis, MO) and then digested for 60 min at 25°C in DMEM-F12 medium containing 1 mg/ml trypsin (Sigma-Aldrich). The cell suspension was digested and washed several times to eliminate testicular somatic cells. The cells were then counted and cultured at 2.0×10^5 cells/ml in DMEM-F12 medium containing 10% fetal bovine serum (FBS). The cells were harvested at each day for 5 days, and viability was assessed using the Vi-Cell XR cell viability analyzer (Beckman Coulter, Fullerton, CA).

Quantitative mRNA Analysis of Uchl1 and Uchl3 Genes by Real-Time PCR

SYBR Green-based real-time quantitative reverse transcription-polymerase chain reaction (RT-PCR; PRISM 7700 Sequence detection system, ABI, Columbia, MD) was performed [20] in SYBR Green Master mix using the following primers: *Uchl1*, 5′-TTCTGTTCAACAACGTGGAC G-3′ and 5′-TCACTGGAAAGGGCATTCG-3′; *Uchl3*, 5′-TGAAGGTC AGACTGAGGCACC-3′ and 5′-AATTGGAAATGGTTTCCGTCC-3′; β-actin, 5′-CGTGCGTGACATCAAAGAGAA-3′ and 5′-CAATAGTGAT-GACCTGGCCGT-3′ To compare *Uchl1* and *Uchl3* gene expression in the first round of spermatogenesis, the formula 2^{-ddCt} was used to calculate relative expression compared with testes of 7-day-old mice.

Western Blotting

Western blots were performed as previously reported [19, 22]. Total protein (5 μg/lane) was subjected to SDS-polyacrylamide gel electrophoresis using 15% gels (Perfect NT Gel, DRC, Japan). Proteins were electrophoretically transferred to polyvinylidene difluoride membranes (Bio-Rad, Hercules, CA) and blocked with 5% nonfat milk in TBS-T (50 mM Tris base, pH 7.5, 150 mM NaCl, 0.1% [w/v] Tween-20). The membranes were incubated individually with one or more primary antibodies to UCHL1 and UCHL3 (1:1000 dilution; peptide antibodies) [20], Bcl-xL, Bax, TRP53, and inactive caspase-3 (1:1000 dilution; all from Cell Signaling Technology, Beverly, MA). Blots were further incubated with peroxidase-conjugated goat anti-mouse IgG or goat anti-rabbit IgG (1:5000 dilution; Pierce, Rockford, IL) for 1 h at room temperature. Immunoreactions were visualized using the SuperSignal West Dura Extended Duration Substrate (Pierce) and analyzed using a ChemiImager (Alpha Innotech, San Leandro, CA).

Sperm Motility, Morphology, and Immunohistochemical Assessments

Sperm were collected from the right cauda epididymidis [27] of 10-wk-old wild-type and *gad* mice in 400 μl human tubal fluid medium containing 0.5% bovine serum albumin and then incubated at 37°C under 5% CO_2 in air for 1–2 h. Using a computer-assisted semen analysis system (TOX IVOS, Hamilton Throne Research, Beverly, MA) [28], sperm were analyzed for the following motion parameters: percentage of motile sperm (MSP), percentage of progressively motile sperm (PMP), average path velocity (VAP), straight-line velocity (VSL), curvilinear velocity (VCL), lateral head displacement (ALH), linearity (VSL/VCL × 100), and straightness (VSL/VAP × 100). All procedures were performed at 37°C. To study the spermatozoa morphology, sperm were smeared and then evaluated for defects in the head, midpiece, and principal piece and for head detachment. For immunocytochemical staining, the sections were incubated with antibodies against UCHL1 (1:1000 dilution; peptide antibody) [20] and ubiquitin (1:500 dilution; DakoCytomation, Glostrup, Denmark) overnight at 4°C in PBS containing 1% BSA.

Statistical Analysis

The mean and standard deviation were calculated for all data (presented as mean ± SD). One-way analysis of variance (ANOVA) was used for all statistical analyses.

RESULTS

Expression of UCHL1 During the First Round of Spermatogenesis

We used Western blotting to characterize the level of UCHL1 and UCHL3 expression in testes from immature wild-type and *gad* mice (Fig. 1, B and C). In agreement with previous data [20], UCHL1 expression was significantly elevated on Day 14 in testicular lysates obtained from 7-, 14-, 21-, 28-, and 35-day-old wild-type mice. The level of UCHL3 expression increased with age and did not differ between *gad* and wild-type mice (Fig. 1B), suggesting that UCHL3 expression is regulated independently of UCH-L1 during the first round of spermatogenesis [20]. We also assessed the expression pattern of *Uchl1* and *Uchl3* genes during juvenile spermatogenesis using SYBR Green-

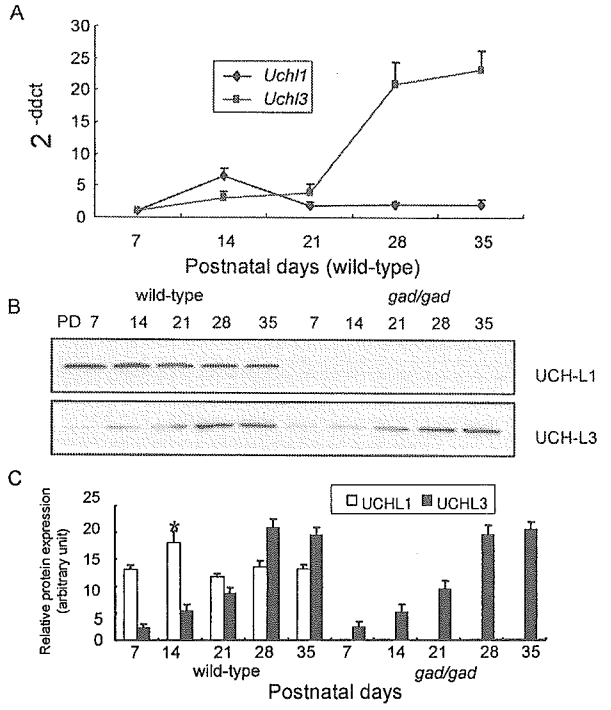

FIG. 1. Expression of UCHL1 and UCHL3during the first round of spermatogenesis. **A**) Comparison of *Uchl1* and *Uchl3* gene expression levels (2^{-ddCt}) by SYBR Green-based real-time quantitative reverse transcription-polymerase chain reaction (RT-PCR). The value for gene expression from the testes of 7-day-old mice was set to 1.0. **B**) Comparison of UCHL1 and UCHL3 expression by Western blotting of testicular lysates from wild-type or *gad* mice. Blots were reprobed for α-tubulin, which was used to normalize the protein load. Representative images from four independent experiments are shown. **C**) Quantitative analysis of changes in UCHL1 and UCHL3 levels by Western blotting. Relative protein expression (optical density) of the bands in panel **B**, normalized to α-tubulin. Each data point represents the mean ± SD (n = 4; * $P < 0.05$).

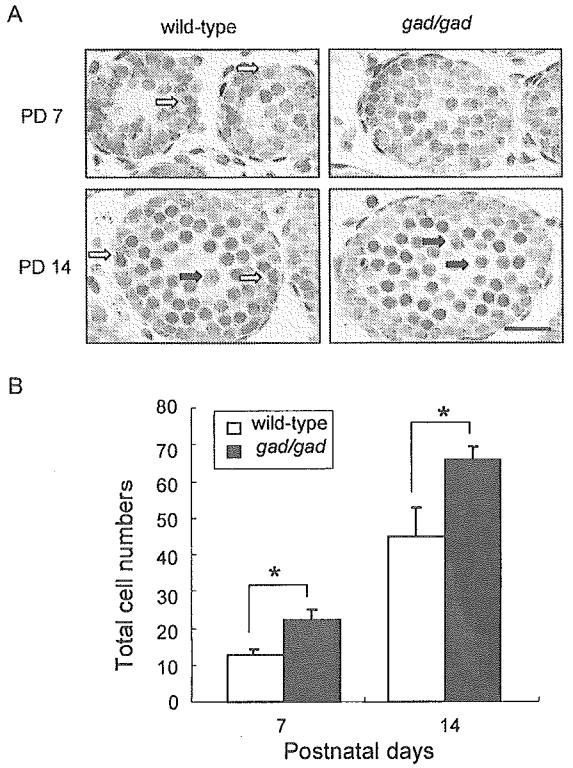

FIG. 2. **A**) Immunohistochemistry of UCHL1 and testicular morphology during the first round of spermatogenesis. UCHL1-positive germ cells in wild-type mice are indicated by open arrows. Spermatogonia and preleptotene spermatocytes (closed arrows) were more abundant and found further from the basement membrane in Postnatal Day (PD) 7 and 14 *gad* mice. Magnification ×200. Bar = 20 μm. **B**) The total number of germ cells in seminiferous tubules was significantly increased in and 7- and 14-day-old *gad* mice compared with wild-type mice (n = 4; * $P < 0.05$). Data represent mean ± SD.

based real-time quantitative RT-PCR (Fig. 1A). Despite the fact that the percentage of spermatogonia and Sertoli cells may be diluted by meiotic and postmeiotic germ cells after Day 14 [20], *Uchl1* expression was high in 14-day-old mice, in agreement with our previous findings.

Immunohistochemistry of UCHL1 and Quantitative Morphometric Assessment

Immunohistochemical analysis revealed UCHL1 expression in spermatogonia from wild-type mice but not *gad* mice (Fig. 2A). Preliminary examination of tubules from immature testes revealed an overproduction of germ cells in *gad* mice. At 7 and 14 days of age, the number of spermatogonia and preleptotene spermatocytes was significantly increased in *gad* mice compared with wild-type mice (Fig. 2A). The increase in the number of these cell types was further confirmed by quantitative analysis, which showed that the total number of testicular cells, including Sertoli cells, was significantly higher in 7- and 14-day-old *gad* mice (Fig. 2B).

TUNEL Staining of Apoptotic Germ Cells During the First Round of Spermatogenesis

To further investigate the mechanism underlying the observed differences in testicular cell numbers between wild-type and *gad* mice during the first round of spermatogenesis, we examined germ cell apoptosis in tissue sections from mice at 7, 14, 21, 28, and 35 days of age by TUNEL assay. During the first round of spermatogenesis, the total number of apoptotic cells in 20 circular seminiferous tubules decreased significantly (n = 4; $P < 0.05$) in gad mouse testes as compared with wild-type mice (Fig. 3A). Although germ cell apoptosis significantly increased at Day 14 in the testes of both wild-type and *gad* mice, *gad* mice had significantly fewer apoptotic germ cells (n = 4; $P < 0.05$) in seminiferous tubules (Fig. 3B).

Testicular Germ Cells of gad *Mice Are Resistant to Apoptosis-Inducing Conditions In Vitro*

Sertoli cells, which support germ cells, express UCHL1 [12]. To explore the viability of germ cells independently of the effect of Sertoli cells, testicular germ cells from 2-wk-old wild-type and *gad* mice were cultured in suspension for 5 days in the presence of 10% FBS. We then examined the resistance of these in vitro cell culture to apoptosis-inducing conditions. Although both wild-type and *gad* mouse cells were sensitive to apoptosis-inducing conditions, the *gad* mouse cells had comparatively greater viability (Fig. 4). Overall results clearly show that the absence of UCHL1 increase germ cell survival.

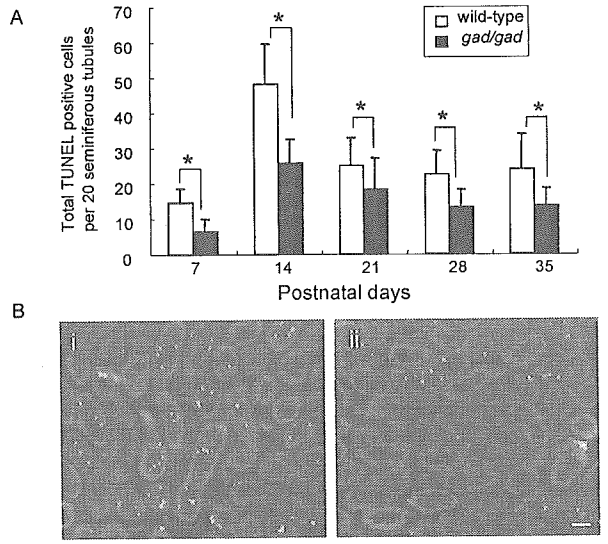

FIG. 3. A) The total TUNEL-positive germinal cells per 20 circular seminiferous tubules in wild-type and *gad* mice on various postnatal days. In each group, the data represent the mean ± SD (n = 4; * $P < 0.05$). B) The extent of apoptosis in 2-wk-old mice. i, wild-type mice; ii, *gad* mice. Green fluorescence, TUNEL-positive cells; red fluorescence, nuclei stained with propidium iodide. Magnification ×100. Bar = 30 μm.

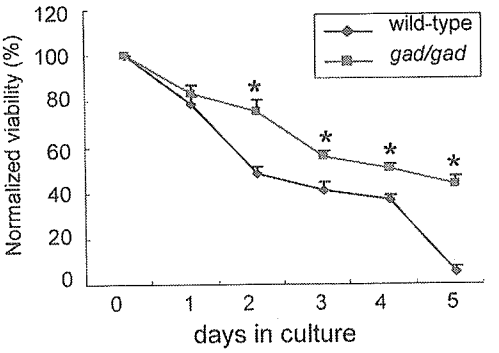

FIG. 4. In vitro survival of testicular germ cells. Testicular germ cells were isolated from wild-type and *gad* mice at 14 days of age. After culture, viability was determined using a Vi-Cell XR cell viability analyzer (Beckman Coulter). Viability at each time point was normalized to that at Day 0. Each data point represents the mean ± SD (n = 4; * $P < 0.05$).

Levels of Apoptotic Proteins During the First Round of Spermatogenesis

Germ cell apoptosis involves genes encoding various factors, such as *Trp53*, the *Bcl2* family, and *caspase*, which are targets for ubiquitination [29–31]. Our previous work demonstrated that the expression of antiapoptotic proteins (Bcl2 family and XIAP) is significantly elevated following cryptorchid stress in *gad* mice [22]. To explore whether the germ cell apoptotic wave is associated with changes in the levels of proteins known to be associated with cell death or survival, Western blot analysis was performed on testicular lysates obtained from 7-, 14-, 21-, 28-, and 35-day-old wild-type and *gad* mice (Fig. 5). Levels of TRP53 and Bax proteins were strikingly elevated in 7-day-old mice but barely detectable on Day 35. Caspase-3 was also strikingly elevated in 7-day-old mice. Since TRP53 modulates Bax expression [22, 32], the observed up-regulation of Bax is consistent with elevated TRP53 levels during the early apoptotic wave. Expression of the antiapoptotic protein Bcl-xL was weaker in immature compared with mature testes. Levels of TRP53, Bax, and caspase-3 proteins were significantly decreased in 7- and 14-day-old *gad* mice relative to the levels observed in wild-type testes (Fig. 5B). By contrast, the level of Bcl-xL protein appeared to be up-regulated earlier in *gad* mice (at 28 days) than in wild-type mice (at 35 days) (Fig. 5B).

Assessment of Cauda Epididymidis and Spermatozoa Morphology in gad *Mice*

The cauda epididymidis from wild-type and *gad* mice were weighed, and the sperm were collected and analyzed. The cauda epididymidis from *gad* mice weighed significantly less, likely resulting from the lower sperm concentration measured in *gad* mice (19.5×10^6/ml) compared with wild-type mice (23.6×10^6/ml) (Table 1). Furthermore, abnormal sperm morphology, including head and midpiece defects or a detached head, occurred significantly more often in *gad* mice (Table 1 and Fig. 6A). Immunocytochemical analysis showed that UCHL1 and ubiquitin were expressed in defective spermatozoa but not in normal spermatozoa (Fig. 6B). Ubiquitin, a marker for sperm abnormalities [33], was detected mainly in defective spermatozoa. However, despite a significantly elevated number of defective spermatozoa, ubiquitin expression in *gad* mouse spermatozoa was similar to that in wild-type mice (data not shown).

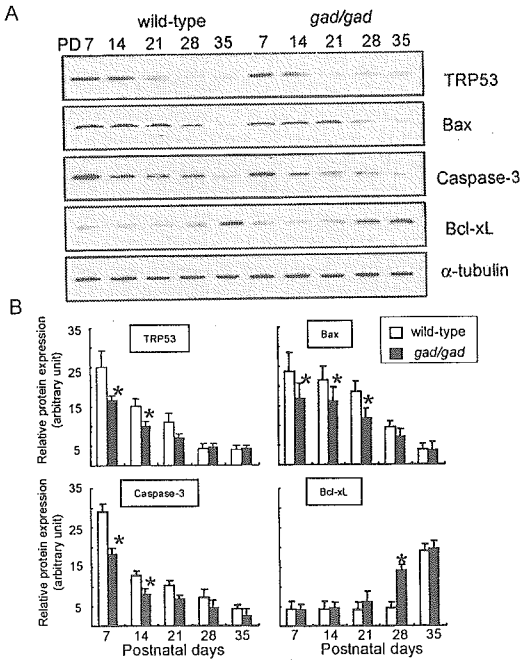

FIG. 5. A) Western blot analyses showing TRP53, Bax, caspase-3, and Bcl-xL levels in wild-type and *gad* mice during the first round of spermatogenesis. Protein (5 μg/lane) was prepared from whole testes at 7, 14, 21, 28, and 35 days of age. Blots were reprobed for α-tubulin to normalize for differences in the amount of protein loaded. Representative images of four independent experiments are shown. B) Quantitative Western blot analysis of changes in TRP53, Bax, caspase-3, and Bcl-xL levels. Relative protein expression (optical density) of the bands in panel A, normalized to α-tubulin. Each data point represents the mean ± SD (n = 4; * $P < 0.05$).

TABLE 1. Analysis of epididymal tail weight and sperm morphology (mean ± SD) in 10-week-old wild-type and *gad* mice.

	Tail weight (mg)	Sperm concentration (10^6/ml)	Defect (%)			
			Head	Midpiece	Principal piece	Detached head
wild-type	30.0 ± 0.8	23.6 ± 3.7	7.2 ± 1.5	2.4 ± 1.3	1.1 ± 0.2	2.0 ± 1.0
gad/gad	24.7 ± 1.1*	19.5 ± 3.3*	14.1 ± 2.8*	4.7 ± 1.5*	1.7 ± 0.6	3.7 ± 1.2*

* Significantly different from wild-type mice (n = 7; $P < 0.05$).

Spermatozoa Motility in gad *Mice*

We measured sperm motility parameters in wild-type and *gad* mice. Of the parameters assessed, MSP, PMP, VAP (μm/sec), VSL (μm/sec), and VCL (μm/sec) were significantly lower in *gad* mice. ALH (μm), linearity (%), and straightness (%) did not differ significantly between *gad* and wild-type mice (Fig. 7). Of the parameters we measured, the number of PMP differed most significantly between *gad* mice (24.4%) and wild-type mice (34.3%) (Fig. 7A).

DISCUSSION

Spermatogenesis is a highly complex process involving male germ cell proliferation and maturation from spermatogonia to spermatozoa [34]. Apoptosis is common during this process and is believed to play an important role in controlling germ cell numbers and eliminating defective germ cells that carry DNA mutations, thus ensuring the production of intact, functional spermatozoa [35–37]. Normally, germ cells are extremely sensitive to DNA damage, as such lesions are incompatible with the ultimate function of these cells [23, 24, 37]. The early apoptotic wave may result in early elimination of defective germ cells in which DNA alterations have occurred through chromosomal crossing over during the first meiotic division [23, 24, 37].

Several lines of evidence indicate that UCHL1 associates with monoubiquitin and that the monoubiquitin pool is reduced in *gad* mice relative to wild-type mice [18, 19, 22]. Furthermore, testes from UCHL1-deficient *gad* mice [22] and mice carrying the K48R mutation in ubiquitin [38] show resistance to cryptorchid-induced apoptosis, suggesting that ubiquitin is critical for modulating testicular germ cell death. Normally, damaged proteins are polyubiquitinated and degraded via the ubiquitin-proteasome system; however, if damaged proteins are not degraded as easily when monoubiquitin is either mutated or reduced [22, 38], then germinal cells may become resistant to programmed death. Our results with the *gad* mouse suggest that ubiquitin induction is important for regulating programmed germinal cell death that is normally observed during the first round of spermatogenesis. We have now shown that immature testes from *gad* mice are resistant to the massive wave of germinal cell apoptosis during the first round of spermatogenesis. The increased resistance of UCHL1-deficient germ cells to apoptosis-inducing conditions in vivo and in vitro suggests that UCHL1 is involved in spermatogenesis (Figs. 3 and 4). The activity of the ubiquitin-proteasome system may be required for specific transitions between multiple developmental cellular processes and sequential apoptosis during spermatogenesis [6, 7, 39]. In addition, the ubiquitin-proteasome system is required for the degradation or modification of numerous germ cell-specific proteins during different phases of spermatogenesis [39–41].

Early apoptosis in testicular germ cells is regulated by a complicated signal transduction pathway. The testes contain high levels of TRP53, Bcl2 family, and caspase-3 proteins, which are targets for ubiquitination [29–31, 42–45]. However, the involvement of the ubiquitin system in the regu-

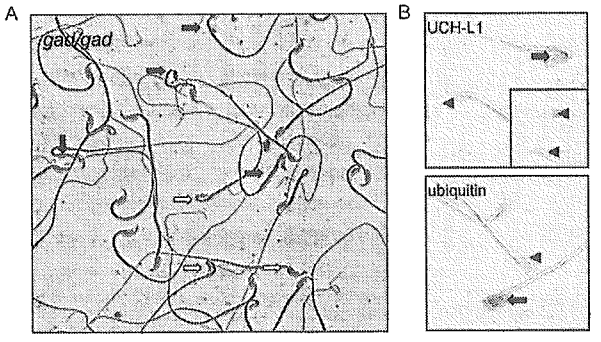

FIG. 6. **A)** Abnormal morphology of spermatozoa from *gad* mice. Spermatozoa were collected from the cauda epididymidis of 10-wk-old *gad* mice. Head defects (open arrows) and midpiece defects (closed arrows) are indicated. Magnification ×400. **B)** Immunocytochemistry of UCH-L1 and ubiquitin in wild-type and *gad* mice. UCHL1- and ubiquitin-positive spermatozoa (closed arrows) and normal spermatozoa (both negative, arrowheads) in wild-type mice are indicated. The inset shows an the image of spermatozoa from *gad* mice. Magnification ×1000.

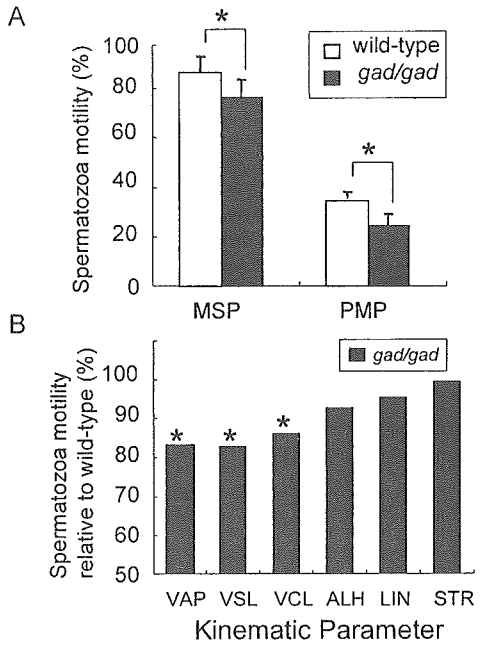

FIG. 7. Kinematic analysis of spermatozoa from the cauda epididymidis of 10-week-old wild-type and *gad* mice. **A)** Sperm motility. MSP, Percentage of motile sperm; PMP, Percentage of progressively motile sperm (n = 7; * $P < 0.05$). Data represent the mean ± SD. **B)** Movement characterization. VAP, Average path velocity (μm/sec); VSL, Straight-line velocity (μm/sec); VCL, Curvilinear velocity (μm/sec); ALH, Lateral head displacement (μm); LIN, Linearity (VSL/VCL × 100); STR, Straightness (VSL/VAP × 100). Data are expressed as a percentage of the values obtained for each parameter in wild-type mice (n = 7; * $P < 0.05$).

latory mechanisms of germ cell apoptosis has not been identified. A previous study showed that UCHL1-deficient *gad* mice express high levels of antiapoptotic proteins (Bcl2 family and XIAP) in the testis following cryptorchid-induced stress [22]. Alterations in the carefully maintained balance between the expression of apoptosis-inducing and apoptosis-protecting proteins may constitute one mechanism underlying the suppression of germ cell apoptosis observed in *gad* mice [46]. The decreased levels of TRP53, Bax, and caspase-3 observed in *gad* mice in this study are consistent with the suppression of germ cell apoptosis. In addition, the expression of the antiapoptotic protein Bcl-xL increased earlier in *gad* mice compared with wild-type mice. Therefore, the control of the apoptotic wave probably depends on variations in the balance between Bax and Bcl-xL [23, 47]. Analysis of the first round of spermatogenesis over time demonstrated a striking and massive wave of apoptotic germinal cells in 14-day-old mice (Fig. 3). High levels of UCHL1 protein were also observed at this age (Fig. 1) [20]. This early apoptotic wave was suppressed in the testes of *gad* mice, which had an abundance of germ cells compared with wild-type mice (Fig. 2). Moreover, the suppression of germ cell death is consistent with our previous report on cryptorchid stress injury in *gad* mice [22]. The testes of *gad* mice showed a phenotype similar to that of *Bax*-deficient mice or those overexpressing *Bcl2* or *Bcl-xL* [23, 25, 26]. Also, the testes of *Trp53*$^{-/-}$ mice exhibited a similar phenotype involving decreased germ cell apoptosis and an increased number of germ cells [48].

In the present study, we also characterized spermatozoa in *gad* mice with regard to the following reproductive endpoints: 1) the weight of reproductive organs, 2) the concentration of sperm cells, and 3) the motility and morphology of spermatozoa collected from the cauda epididymidis. The weight of cauda epididymidis from *gad* mice was significantly lower compared with that from wild-type mice. The concentration of sperm cells was also significantly lower, and most motility parameters of spermatozoa collected from the cauda epididymidis were affected in *gad* mice (Fig. 7). The significant decline in progressive forward motility, VAP, VSL, and VCL indicates that UCHL1 deficiency affects not only the ability of spermatozoa to move in the forward direction but also their vigor. In addition, the percentage of morphologically abnormal spermatozoa was significantly higher in *gad* mice (Table 1 and Fig. 6A).

Sperm production in the testis is a regulated balance between germ cell division and germ cell loss [26, 49], and there is emerging evidence that the ubiquitin-proteasome system may be central to the coordination of this process. For example, during spermatogenesis, the general activity of the ubiquitin-proteasome system is high, probably reflecting the requirement for massive degradation of cytoplasmic and nuclear proteins [6, 7, 50, 51]. Additionally, mutation of the ubiquitin-conjugating enzyme HR6B results in impaired spermatogenesis during nuclear condensation in spermatids [39, 41]. We found the fact that UCH-L1 associates with monoubiquitin in several lines of *gad* mice [18, 19, 22]. Furthermore, both proteins are expressed abundantly and at comparable levels in testis and the epididymis [11, 13, 14], suggesting that the functions of two proteins are important during spermatogenesis. Ubiquitin is present in defective spermatozoa, and proteins in these cells become ubiquitinated during epididymal passage (Fig. 6B) [11, 14, 33, 52, 53]. Furthermore, ubiquitination in the epididymis may trigger apoptotic mechanisms that recognize and eliminate abnormal spermatozoa [49, 54, 55].

Further study is required to elucidate the functional significance of the association between UCHL1 and ubiquitin during spermatozoa maturation in the epididymis. However, our observations suggest that UCHL1 may function to regulate sperm production and to ubiquitinate proteins in defective spermatozoa. Our present study demonstrates that UCHL1-deficient *gad* mice are resistant to the wave of germinal cell apoptosis that occurs during the first round of spermatogenesis and that these mice have defects in sperm production, motility, and morphology. These results suggest that UCHL1 functions in the early apoptotic wave during the first round of spermatogenesis and in the control of sperm quality during sperm maturation.

ACKNOWLEDGMENTS

We thank H. Kikuchi for technical assistance with tissue sections and M. Shikama for the care and breeding of animals.

REFERENCES

1. Ciechanover A, Finley D, Varshavsky A. Ubiquitin dependence of selective protein degradation demonstrated in the mammalian cell cycle mutant ts85. Cell 1984; 37:57–66.
2. Glotzer M, Murray AW, Kirschner MW. Cyclin is degraded by the ubiquitin pathway. Nature 1991; 349:132–138.
3. Strous GJ, Govers R. The ubiquitin-proteasome system and endocytosis. J Cell Sci 1999; 112(pt 10):1417–1423.
4. Wilkinson KD. Regulation of ubiquitin-dependent processes by deubiquitinating enzymes. FASEB J 1997; 11:1245–1256.
5. Hershko A, Ciechanover A. The ubiquitin system. Annu Rev Biochem 1998; 67:425–479.
6. Baarends WM, Roest HP, Grootegoed JA. The ubiquitin system in gametogenesis. Mol Cell Endocrinol 1999; 151:5–16.
7. Baarends WM, van der Laan R, Grootegoed JA. Specific aspects of the ubiquitin system in spermatogenesis. J Endocrinol Invest 2000; 23:597–604.
8. Ciechanover A. The ubiquitin-proteasome pathway: on protein death and cell life. EMBO J 1998; 17:7151–7160.
9. Weissman AM. Themes and variations on ubiquitylation. Nat Rev Mol Cell Biol 2001; 2:169–178.
10. Wing SS. Deubiquitinating enzymes—the importance of driving in reverse along the ubiquitin-proteasome pathway. Int J Biochem Cell Biol 2003; 35:590–605.
11. Fraile B, Martin R, De Miguel MP, Arenas MI, Bethencourt FR, Peinado F, Paniagua R, Santamaria L. Light and electron microscopic immunohistochemical localization of protein gene product 9.5 and ubiquitin immunoreactivities in the human epididymis and vas deferens. Biol Reprod 1996; 55:291–297.
12. Kon Y, Endoh D, Iwanaga T. Expression of protein gene product 9.5, a neuronal ubiquitin C-terminal hydrolase, and its developing change in sertoli cells of mouse testis. Mol Reprod Dev 1999; 54:333–341.
13. Kwon J, Kikuchi T, Setsuie R, Ishii Y, Kyuwa S, Yoshikawa Y. Characterization of the testis in congenitally ubiquitin carboxy-terminal hydrolase-1 (Uch-L1) defective (gad) mice. Exp Anim 2003; 52:1–9.
14. Martin R, Santamaria L, Fraile B, Paniagua R, Polak JM. Ultrastructural localization of PGP 9.5 and ubiquitin immunoreactivities in rat ductus epididymidis epithelium. Histochem J 1995; 27:431–439.
15. Pickart CM, Rose IA. Ubiquitin carboxyl-terminal hydrolase acts on ubiquitin carboxyl-terminal amides. J Biol Chem 1985; 260:7903–7910.
16. Liu Y, Fallon L, Lashuel HA, Liu Z, Lansbury PT, Jr. The UCH-L1 gene encodes two opposing enzymatic activities that affect alpha-synuclein degradation and Parkinson's disease susceptibility. Cell 2002; 111:209–218.
17. Liu Y, Lashuel HA, Choi S, Xing X, Case A, Ni J, Yeh LA, Cuny GD, Stein RL, Lansbury PT, Jr. Discovery of inhibitors that elucidate the role of UCH-L1 activity in the H1299 lung cancer cell line. Chem Biol 2003; 10:837–846.
18. Osaka H, Wang YL, Takada K, Takizawa S, Setsuie R, Li H, Sato Y, Nishikawa K, Sun YJ, Sakurai M, Harada T, Hara Y, Kimura I, Chiba S, Namikawa K, Kiyama H, Noda M, Aoki S, Wada K. Ubiquitin carboxy-terminal hydrolase L1 binds to and stabilizes monoubiquitin in neuron. Hum Mol Genet 2003; 12:1945–1958.

19. Harada T, Harada C, Wang YL, Osaka H, Amanai K, Tanaka K, Takizawa S, Setsuie R, Sakurai M, Sato Y, Noda M, Wada K. Role of ubiquitin carboxy terminal hydrolase-L1 in neural cell apoptosis induced by ischemic retinal injury in vivo. Am J Pathol 2004; 164:59–64.
20. Kwon J, Wang YL, Setsuie R, Sekiguchi S, Sakurai M, Sato Y, Lee WW, Ishii Y, Kyuwa S, Noda M, Wada K, Yoshikawa Y. Developmental regulation of ubiquitin C-terminal hydrolase isozyme expression during spermatogenesis in mice. Biol Reprod 2004; 71:515–521.
21. Saigoh K, Wang YL, Suh JG, Yamanishi T, Sakai Y, Kiyosawa H, Harada T, Ichihara N, Wakana S, Kikuchi T, Wada K. Intragenic deletion in the gene encoding ubiquitin carboxy-terminal hydrolase in gad mice. Nat Genet 1999; 23:47–51.
22. Kwon J, Wang YL, Setsuie R, Sekiguchi S, Sato Y, Sakurai M, Noda M, Aoki S, Yoshikawa Y, Wada K. Two closely related ubiquitin C-terminal hydrolase isozymes function as reciprocal modulators of germ cell apoptosis in cryptorchid testis. Am J Pathol 2004; 165: 1367–1374.
23. Rodriguez I, Ody C, Araki K, Garcia I, Vassalli P. An early and massive wave of germinal cell apoptosis is required for the development of functional spermatogenesis. EMBO J 1997; 16:2262–2270.
24. Jahnukainen K, Chrysis D, Hou M, Parvinen M, Eksborg S, Soder O. Increased apoptosis occurring during the first wave of spermatogenesis is stage-specific and primarily affects midpachytene spermatocytes in the rat testis. Biol Reprod 2004; 70:290–296.
25. Furuchi T, Masuko K, Nishimune Y, Obinata M, Matsui Y. Inhibition of testicular germ cell apoptosis and differentiation in mice misexpressing Bcl-2 in spermatogonia. Development 1996; 122:1703–1709.
26. Russell LD, Chiarini-Garcia H, Korsmeyer SJ, Knudson CM. Bax-dependent spermatogonia apoptosis is required for testicular development and spermatogenesis. Biol Reprod 2002; 66:950–958.
27. Slott VL, Suarez JD, Perreault SD. Rat sperm motility analysis: methodologic considerations. Reprod Toxicol 1991; 5:449–458.
28. Goyal HO, Braden TD, Mansour M, Williams CS, Kamaleldin A, Srivastava KK. Diethylstilbestrol-treated adult rats with altered epididymal sperm numbers and sperm motility parameters, but without alterations in sperm production and sperm morphology. Biol Reprod 2001; 64:927–934.
29. Chipuk JE, Green DR. Cytoplasmic p53: Bax and forward. Cell Cycle 2004; 3:429–431.
30. Dimmeler S, Breitschopf K, Haendeler J, Zeiher AM. Dephosphorylation targets Bcl-2 for ubiquitin-dependent degradation: a link between the apoptosome and the proteasome pathway. J Exp Med 1999; 189:1815–1822.
31. Suzuki Y, Nakabayashi Y, Takahashi R. Ubiquitin-protein ligase activity of X-linked inhibitor of apoptosis protein promotes proteasomal degradation of caspase-3 and enhances its anti-apoptotic effect in Fas-induced cell death. Proc Natl Acad Sci U S A 2001; 98:8662–8667.
32. Selvakumaran M, Lin HK, Miyashita T, Wang HG, Krajewski S, Reed JC, Hoffman B, Liebermann D. Immediate early upregulation of bax expression by p53 but not TGF beta 1: a paradigm for distinct apoptotic pathways. Oncogene 1994; 9:1791–1798.
33. Sutovsky P, Moreno R, Ramalho-Santos J, Dominko T, Thompson WE, Schatten G. A putative, ubiquitin-dependent mechanism for the recognition and elimination of defective spermatozoa in the mammalian epididymis. J Cell Sci 2001; 114:1665–1675.
34. de Kretser DM, Loveland KL, Meinhardt A, Simorangkir D, Wreford N. Spermatogenesis. Hum Reprod 1998; 13(suppl 1):1–8.
35. Gosden R, Spears N. Programmed cell death in the reproductive system. Br Med Bull 1997; 53:644–661.
36. Matsui Y. Regulation of germ cell death in mammalian gonads. APMIS 1998; 106:142–147Ascussion 147–148.
37. Print CG, Loveland KL. Germ cell suicide: new insights into apoptosis during spermatogenesis. Bioessays 2000; 22:423–430.
38. Rasoulpour RJ, Schoenfeld HA, Gray DA, Boekelheide K. Expression of a K48R mutant ubiquitin protects mouse testis from cryptorchid injury and aging. Am J Pathol 2003; 163:2595–2603.
39. Baarends WM, Wassenaar E, Hoogerbrugge JW, van Cappellen G, Roest HP, Vreeburg J, Ooms M, Hoeijmakers JH, Grootegoed JA. Loss of HR6B ubiquitin-conjugating activity results in damaged synaptonemal complex structure and increased crossing-over frequency during the male meiotic prophase. Mol Cell Biol 2003; 23:1151–1162.
40. Baarends WM, Hoogerbrugge JW, Roest HP, Ooms M, Vreeburg J, Hoeijmakers JH, Grootegoed JA. Histone ubiquitination and chromatin remodeling in mouse spermatogenesis. Dev Biol 1999; 207: 322–333.
41. Roest HP, van Klaveren J, de Wit J, van Gurp CG, Koken MH, Vermey M, van Roijen JH, Hoogerbrugge JW, Vreeburg JT, Baarends WM, Bootsma D, Grootegoed JA, Hoeijmakers JH. Inactivation of the HR6B ubiquitin-conjugating DNA repair enzyme in mice causes male sterility associated with chromatin modification. Cell 1996; 86: 799–810.
42. Marshansky V, Wang X, Bertrand R, Luo H, Duguid W, Chinnadurai G, Kanaan N, Vu MD, Wu J. Proteasomes modulate balance among proapoptotic and antiapoptotic Bcl-2 family members and compromise functioning of the electron transport chain in leukemic cells. J Immunol 2001; 166:3130–3142.
43. Oren M. Regulation of the p53 tumor suppressor protein. J Biol Chem 1999; 274:36031–36034.
44. Orlowski RZ. The role of the ubiquitin-proteasome pathway in apoptosis. Cell Death Differ 1999; 6:303–313.
45. Yang Y, Yu X. Regulation of apoptosis: the ubiquitous way. FASEB J 2003; 17:790–799.
46. Beumer TL, Roepers-Gajadien HL, Gademan IS, Lock TM, Kal HB, De Rooij DG. Apoptosis regulation in the testis: involvement of Bcl-2 family members. Mol Reprod Dev 2000; 56:353–359.
47. Borner C. The Bcl-2 protein family: sensors and checkpoints for life-or-death decisions. Mol Immunol 2003; 39:615–647.
48. Yin Y, Stahl BC, DeWolf WC. Morgentaler A. p53-mediated germ cell quality control in spermatogenesis. Dev Biol 1998; 204:165–171.
49. Sutovsky P. Ubiquitin-dependent proteolysis in mammalian spermatogenesis, fertilization, and sperm quality control: killing three birds with one stone. Microsc Res Tech 2003; 61:88–102.
50. Rajapurohitam V, Bedard N, Wing SS. Control of ubiquitination of proteins in rat tissues by ubiquitin conjugating enzymes and isopeptidases. Am J Physiol Endocrinol Metab 2002; 282:E739–E745.
51. Rajapurohitam V, Morales CR, El-Alfy M, Lefrancois S, Bedard N, Wing SS. Activation of a UBC4-dependent pathway of ubiquitin conjugation during postnatal development of the rat testis. Dev Biol 1999; 212:217–228.
52. Lippert TH, Seeger H, Schieferstein G, Voelter W. Immunoreactive ubiquitin in human seminal plasma. J Androl 1993; 14:130–131.
53. Sutovsky P, Terada Y, Schatten G. Ubiquitin-based sperm assay for the diagnosis of male factor infertility. Hum Reprod 2001; 16:250–258.
54. Sinha Hikim AP, Swerdloff RS. Hormonal and genetic control of germ cell apoptosis in the testis. Rev Reprod 1999; 4:38–47.
55. Sutovsky P, Hauser R, Sutovsky M. Increased levels of sperm ubiquitin correlate with semen quality in men from an andrology laboratory clinic population. Hum Reprod 2004; 19:628–638.

Available online at www.sciencedirect.com
SCIENCE DIRECT
Neuroscience Research 53 (2005) 241–249
Neuroscience Research
www.elsevier.com/locate/neures

Clinico-pathological rescue of a model mouse of Huntington's disease by siRNA

Yu-Lai Wang [a,b,1], Wanzhao Liu [a,b,1], Etsuko Wada [a], Miho Murata [a,b], Keiji Wada [a,b], Ichiro Kanazawa [a,b,*]

[a] *Department of Degenerative Neurological Diseases, National Institute of Neuroscience, National Center of Neurology and Psychiatry (NCNP), Tokyo 187-8502, Japan*
[b] *Solution Oriented Research for Science and Technology (SORST), Japan Science and Technology Agency (JST), Saitama 332-0012, Japan*

Received 11 January 2005; accepted 28 June 2005
Available online 10 August 2005

Abstract

Huntington's disease (HD) is an autosomal dominant inheritable neurodegenerative disorder currently without effective treatment. It is caused by an expanded polyglutamine (poly Q) tract in the corresponding protein, huntingtin (htt), and therefore suppressing the huntingtin expression in brain neurons is expected to delay the onset and mitigate the severity of the disease. Here, we have used small interfering RNAs (siRNAs) directed against the huntingtin gene to repress the transgenic mutant huntingtin expression in an HD mouse model, R6/2. Results showed that intraventricular injection of siRNAs at an early postnatal period inhibited transgenic huntingtin expression in brain neurons and induced a decrease in the numbers and sizes of intranuclear inclusions in striatal neurons. Treatments using this siRNA significantly prolonged model mice longevity, improved motor function and slowed down the loss of body weight. This work suggests that siRNA-based therapy is promising as a future treatment for HD.

Keywords: Huntington's disease; HD mouse model (R6/2); Small interfering RNAs (siRNAs); Gene therapy

1. Introduction

Huntington's disease (HD) is a choreic-psychiatric neurodegenerative disease that is inherited in an autosomal dominant manner. HD is caused by an expansion of CAG repeats (more than 35) in the HD gene, yielding an expanded polyglutamine (poly Q) tract in the protein, huntingtin (htt) (Gusella and MacDonald, 2000). Pathologically, HD is characterized by selective loss of brain neurons and the formation of intranuclear aggregates (inclusion bodies) composed of htt and other functional proteins in the remaining neurons (Hazeki et al., 2002; Busch et al., 2003). Transgenic mice with human htt exon 1 containing expanded CAG repeats displayed abnormal behavior as well as ubiquitinated neuronal intranuclear inclusions (NIIs) composed of poly Q aggregations found in the striatal and cortical neurons, revealing that mutant htt exon 1 is sufficient to cause the disease (Mangiarini et al., 1996). There is, however, a controversy as to whether NIIs are harmful to living cells or act in their defense by sequestering toxic soluble mutant htt (Kaytor et al., 2004). In this regard, there is a general consensus that cytosolic mutant htt forms invisible or minute aggregates that adversely affect cell survival (Trushina et al., 2003) through dysregulation or upregulation of CRE-mediated transcription (Gines et al., 2003; Obrietan and Hoyt, 2004; Sugars et al., 2004). All of these findings suggest that the expression of the mutant huntingtin may cause the disease via a "gain-of-function" mechanism. Down-regulation of mutant huntingtin expression has been suggested to be a promising therapeutic strategy (Haque et al., 1997). Yamamoto et al. (2000), using a conditional mouse model of HD,

* Corresponding author. Tel.: +81 42 3461780; fax: +81 42 3461762.
E-mail address: ichiro@ncnp.go.jp (I. Kanazawa).
[1] Both these authors contributed equally to this work.

0168-0102/$ – see front matter © 2005 Elsevier Ireland Ltd and the Japan Neuroscience Society. All rights reserved.
doi:10.1016/j.neures.2005.06.021

demonstrated that "switching off" the transgenic htt expression at the adult age would lessen the severity of the disease, suggesting that HD might be reversible. Thus, we expected that suppression of mutant htt gene expression in brain neurons would constitute a reasonable clinical approach to combat HD.

Several techniques have been explored to block the expression of huntingtin expression, including antisense technology (Boado et al., 2000; Nellemann et al., 2000) and catalytic DNA (Yen et al., 1999). Small interfering RNAs (siRNAs) offer a much more powerful means to selectively silence genes by base-pairing in mammalian somatic cells, and these RNAs are very specific, stable and highly efficient. Recently, we have identified highly effective and specific siRNAs against huntingtin exon 1 mRNA using cell culture models (Liu et al., 2003). Here, we delivered these siRNAs into brain neurons of newborn HD transgenic mice (R6/2) to test whether the model mice can benefit from siRNA treatment.

2. Materials and methods

2.1. HD model mouse

HD transgenic mice (R6/2) were purchased from Jackson Laboratory (Bar Harbor, Maine). The strain was maintained by crossing ovarian transplant hemizygote females with wild-type B6CBAF1/J males following the protocol of Jackson Laboratory. The HD transgene comprises about 1 kb of the human HD gene and includes the promoter, 5′ untranslated region (5′ UTR), and exon 1 with 144 CAG repeats (Mangiarini et al., 1996). Offsprings were genotyped by PCR using tail tip total genomic DNA following the protocol of Jackson Laboratory. Because the highly expanded CAG repeats are unstable in transgenic mice, especially on paternal transmission (Mangiarini et al., 1997), we used only F1 generation in this work. All the mutant htt transgenic mice (half in F1 generation) used here have a transgenic mutant htt allele with same or nearly same CAG repeat number. The wild-type littermates, B6CBAF1/J, were used as controls. The mice were housed one to five per cage with food and water available. Animal care and handling were in accordance with institutional regulations for animal care and were approved by the Animal Investigation Committee of the National Institute of Neuroscience, NCNP, Japan.

2.2. siRNAs

Single-stranded 21-nt RNAs (siRNA-HDExon1, sense strand, 5′-GCCUUCGAGUCCCUCAAGUCC-3′; antisense strand, 3′-UCCGGAAGCUCAGGGAGUUCA-5′) were custom synthesized and HPLC-purified (Qiagen, Huntsville, AL) and annealed as described previously (Liu et al., 2003). A non-silencing siRNA was used as control (Qiagen).

2.3. Cell culture and transfection

Cell lines and the recombinant htt72Q-d1EGFP fusion protein expression vectors were as previously described (Liu et al., 2003). Protocols for cell culture and co-transfection using Lipofectamine 2000 (Invitrogen, Carlsbad, CA) of siRNAs and htt72Q-d1EGFP vectors were same as described previously (Liu et al., 2003). Cos-7, SH-SY5Y and Neuro-2A cell lines were used. Cells were grown in Minimum Essential Medium-Alpha Medium (Gibco BRL) (for Cos-7), or in Dulbecco's Modified Eagle's Medium (Gibco BRL) (for SH-SY5Y and Neuro-2A) supplemented with 10% heat-inactivated fetal bovine serum (FBS, Mitsubishi Kasei) and antibiotics (10 units/ml of penicillin and 50 μg/ml of streptomycin; Meiji). A 12-well plate was used to perform co-transfection experiments of httQ72-d1EGFP and siRNAs. Forty eight hours after co-transfection, cultured plates were observed under fluorescence microscopy to examine the expression level and the distribution of fused huntingtin-EGFP proteins.

2.4. In vivo transfection

To test the silencing effects of siRNAs, we cotransfected httQ72-d1EGFP and siRNAs into new-born mouse (wild-type, P2) brain neurons using ExGen 500 that is designed for in vivo transfection. We followed the manufacturer's protocols and adjusted the ExGen 500/(vectors + siRNAs) ratio (N/P ratio) to 6, and injected 5 μl of the solution containing 0.25 μg of httQ72-d1EGFP and 0.2 μg of siRNAs. Mice were sacrificed 96 h after transfection, and brain tissues were taken out and sectioned to examine under fluorescence microscopy.

To evaluate their efficiency of siRNAs delivery and cytotoxicity in vivo, two commercially available transfection reagents, Lipofectamine 2000 (Invitrogen) and ExGen 500 (Fermentas, Hanover, MD) were tested in wild-type mice. In experiments using ExGen 500, we followed the manufacturer's protocols and adjusted the ExGen 500/siRNA ratio (N/P ratio) to 6, and 5 μl of transfection solution was applied for each mouse. When using Lipofectamine 2000, each mouse received about 5 μl of transfection complex solution containing 0.2 μg siRNAs and 0.5 μl Lipofectamine 2000. A 10 μl microsyringe was used to inject the transfection complex solution. The delivery efficiency of ExGen 500 is very high but it seems it is also more toxic compared to Lipofectamine 2000 (data not shown). The cytotoxicity caused by Lipofectamine reagent seems very minor in P2 mice brain, but perhaps its delivery efficiency is lower than ExGen 500. Finally, we chose the Lipofectamine 2000 reagent to deliver siRNA. The three experimental controls: buffer-treated, control siRNA-treated and untreated were used. For each newborn (P2) mouse, transfection solution was directly injected into lateral ventricle to a depth of 2.0 mm approximately at the position of 1 mm to the right of and 1 mm posterior from Bregma, as

previously reported (Shen et al., 2001, 2002; Sakurai et al., 2004). Since there is no suitable method to directly detect the siRNA for histology, 5 μl of Alcian blue dye was injected into normal mice at P2 in order to define the site of injection of the siRNA via histological examination of brain sections. The immediate analysis revealed that in most cases the dye was injected into the lateral ventricle (data not shown). P2 mouse injections were typically made blindly with respect to genotype. About 4 weeks after injection, all genotyping was performed by PCR using genomic DNA from tail biopsies.

2.5. Quantitative RT-PCR

Two to 14 days after injecting the siRNA/transfection complexes, the mice were sacrificed and whole brain tissues were collected ($n = 3$ for each group). Transgenic mRNA was estimated by quantitative RT-PCR using SYBR Green PCR master mix on an ABI 7700 sequence detector. Primers were: forward, 5′-CGCCGCCTCCTCAGCTTCCT-3′ and reverse, 5′-GCGGTGGTGGCGGCGGCGGCT-3′. Expression of GAPDH and β-actin were also estimated in each sample using the same methods as controls.

2.6. Western blot analysis

Protein lysates from the striatum were extracted using NE-PER Nuclear and Cytoplasmic Extraction Reagents (Pierce). Approximately 50 μg of nuclear protein extracts were loaded per lane on 5–10% gradient SDS-PAGE gels. The proteins were electrophoretically transferred to Immobilon-P membranes (0.45 μm, Millipore, Bedford, MA). Primary antibodies were directed against huntingtin (MAB5374, Chemicon, Temecula, CA). Anti-β-actin antibody (Sigma) was used as an internal control. Immunoreactions were visualized using the SuperSignal West Dura Extended Duration Substrate (Pierce, Rockford, IL) and analyzed with a ChemiImager (Alpha Innotech, CA).

2.7. Immunohistochemistry

Brains from mice ($n = 3$ for each group) were fixed in 4% paraformaldehyde (PFA) in phosphate-buffered saline (PBS, pH 7.4) and embedded in paraffin. Sections (4-μm) were used for immunohistochemistry by mouse monoclonal anti-huntingtin antibody (MAB5374, 1:500). Subsequent antibody detection was carried out using anti-mouse IgG from the Vectorstain Elite ABC kit (Vector Labs, Burlingame, CA).

2.8. Assessment of symptoms

2.8.1. Body weight

Body weight was measured weekly for all surviving mice from ages 4 to 17 weeks, including wild-type or transgenic, treated or untreated.

2.8.2. Tail suspension test

Mice over 4 weeks old were suspended by their tails for 15 s, during which the limbs of R6/2 may exhibit a feet-clasping posture not observed in wild-type mice. Mice showing feet-clasping posture during the 15 s suspension were scored positive.

2.8.3. Rotarod test

Forced motor activity was tested with an accelerating rotarod (Ohara, Japan). The mice were placed on the inactive drum and then forced to walk in the forward direction as the drum was accelerated from 3 to 30 rpm over a period of 300 s. The time until the animal fell off the drum was noted, with a cutoff of 300 s. Mice (siRNA-treated: $n = 17$, mock-treated: $n = 10$, untreated: $n = 11$) were tested at 6, 7 and 8 weeks of age. At each time point, the mice were tested on 2 consecutive days, for three trials per day. Data used in statistical analyses were from the second day, since the first day was for the mice to learn the task.

2.8.4. Open-field analysis

The pattern of movement of each mouse was monitored for 10 min in a 50 cm × 50 cm open field chamber (Ohara, Japan) made of gray polyvinyl chloride. The floor of the open field was divided into 25 equal quadrants by 5 cm × 5 cm perpendicular black lines. A video camera was mounted 80 cm above the field and connected to a Macintosh G4 computer. Diffuse white light provided an illumination density of approximately 0.4 lx at the center of the field. The mice were given three training sessions to acclimatize them to the open-field equipment. The mice were placed into the foremost right corner and observed for 10 min. Data for movement trace, distance and positions at a corresponding time were recorded by the computer and analyzed using Image OF 2.03, a modified software program based on the public domain NIH Image program (developed at the U.S. National Institutes of Health and available on the Internet at http://rsb.info.nih.gov/nih-image/). After each trial, the apparatus was cleaned with 70% alcohol.

2.8.5. Survival analysis

The dates of birth and death were recorded for every R6/2 mouse to calculate longevity (days) for each mouse and for a further survival analysis.

3. Results

3.1. Effects of siRNAs on htt expression in vitro and in vivo

We designed a 21-nucleotide siRNA (siRNA-HDExon1, Fig. 1(B)) targeted against the sequence (underlined in red) at immediate upstream of the CAG repeats of human htt (Fig. 1(A), underlined in green). Cultured Cos-7 cells cotransfected with httQ72-d1EGFP and siRNA-HDExon1

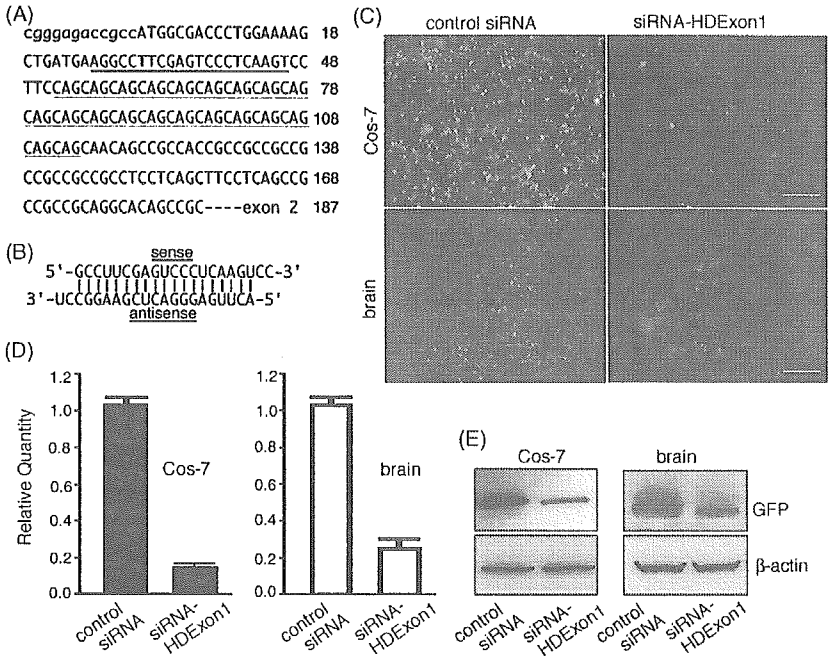

Fig. 1. siRNA-HDExon1 is effective and specific in vivo and in vitro. (A) cDNA sequence showing the target position for siRNA-HDExon1 (red underline) and CAG repeats (green underline) in the first exon of the human huntingtin gene. (B) Sequences and predicted structure for the siRNA-HDExon1. (C) Representative images showing the effects of siRNA-HDExon1 against the httQ72-d1EGFP fusion protein in Cos-7 cells (upper panels) and newborn mouse brain neurons (lower panels), respectively. Scale bar, 200 μm. (D) Quantitative RT-PCR results showing the knock-down of targeted httQ72-d1EGFP mRNA by siRNA-HDExon1 in vitro using cultured Cos-7 cells (left panel), and in vivo by transfection of newborn mouse brain (right panel). (E) Western blots showing down-regulation of the targeted httQ72-d1EGFP fusion protein in Cos-7 cell lysates and brain lysates. β-actin was used as a protein loading control.

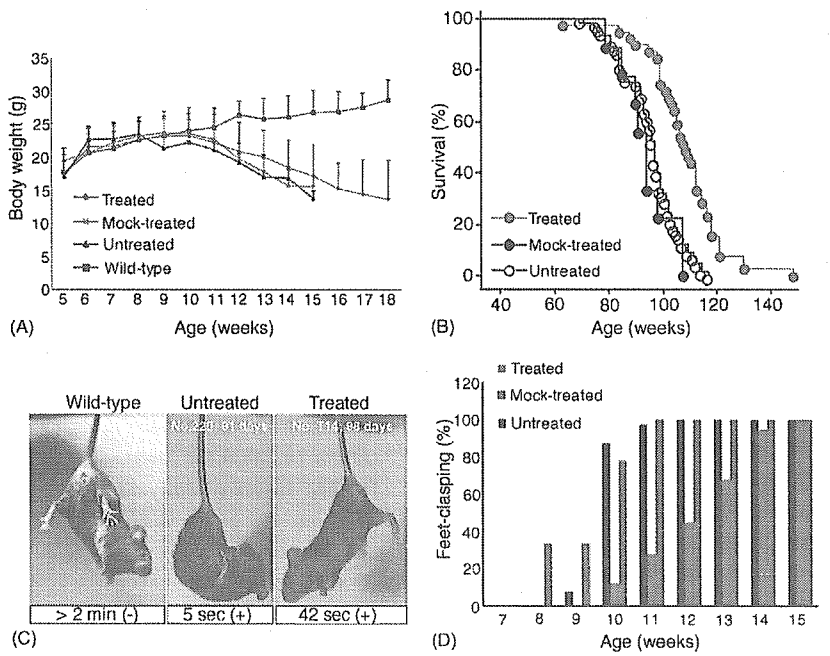

Fig. 2. Effects of siRNA-HDExon1 on the symptomatic phenotypes of the HD mouse model. (A) Effect of siRNA-HDExon1 on body weight in R6/2 mice. Body weight loss was delayed in the siRNA-HDExon1-treated group compared with the mock-treated or untreated groups (statistically significant at 13, 14 and 15 weeks; $p < 0.01$ by ANOVA). Vertical bars indicate S.D. (B) Survival curves (Kaplan–Meier method) showing that siRNA-HDExon1 treatment extended the longevity of R6/2 mice significantly ($p < 0.0001$ by log-rank test; siRNA-treated, $n = 39$; mock-treated, $n = 9$; untreated, $n = 65$). Wild-type mice that had the same treatment had a normal lifespan. (C) Representative images showing the effect of siRNA-HDExon1 on the test for the feet-clasping phenotype during tail suspension. A 13-week-old untreated R6/2 mouse displayed the feet-clasping posture at 5 s (center), whereas a 14-week-old R6/2 mouse treated with siRNA-HDExon1 did not display it until 42 s (right). (D) The treatment of siRNA-HDExon1 significantly delayed the age of feet-clasping (siRNA-treated, $n = 41$; mock-treated, $n = 12$; untreated, $n = 48$). The y-axis of the graph shows the percentage of mice that displayed the feet-clasping posture during the 15 s test period.

showed that the siRNAs efficiently suppressed the expression of recombinant httQ72-d1EGFP, while the control siRNAs (Qiagen, non-silencing control siRNAs) did not affect the expression (Fig. 1(C) upper panels). The suppression was confirmed by quantitative RT-PCR and Western blot analysis. As shown in Fig. 1(D) (left), cells transfected with the siRNA-HDExon1 reduced the expression of cognate htt-EGFP mRNA. Western blots showed a lowered htt-EGFP protein level in siRNA-HDExon1-treated cells (Fig. 1(E), left). Similar results were obtained in experiments using cultured SH-SY5Y and Neuro-2A cells, revealing that the suppressive effects did not differ significantly among cell types (data not shown). Besides, the siRNA-HDExon1 efficiently down-regulated the endogenous htt expression in cultured human cells (Liu et al., 2003).

Since chemically synthesized siRNAs were effective and specific in cell culture models, we then tested whether siRNA-HDExon1 was effective in mouse brain neurons through in vivo cotransfection with httQ72-d1EGFP constructs. Fig. 1(C) (lower panels) showed that siRNA-HDExon1 effectively knocked down the httQ72-d1EGFP expression in newborn mouse brain neurons (Fig. 1(C), lower panels). These effects were also confirmed by quantitative RT-PCR (Fig. 1(D), right), and by Western blots (Fig. 1(E), right). Both htt-EGFP mRNA and protein were suppressed in the mouse treated with siRNA-HDExon1 compared with those treated by a non-silencing control siRNA (Qiagen).

These results indicate that siRNA-HDExon1 is highly effective in HD gene suppression both in vitro and in vivo. We next applied this siRNA to the HD model mouse, R6/2 to test if it is beneficial.

3.2. Effects of siRNAs on HD transgenic model mice, R6/2

3.2.1. Change of body weight

The growth of R6/2 mice was normal before the onset of the HD-like phenotypes caused by transgenic mutant htt exon 1 containing expanded CAG repeats (Mangiarini et al., 1996). From ages 8 to 9 weeks, due to the expression of the transgenic HD exon 1 and subsequent accumulation of mutant htt, R6/2 mice had an obviously smaller body size compared with age-matched wild-type mice. Deaths occurred at 14–15 weeks of age with a significant loss of body weight. We analyzed the body weight change in line with ages (weeks) among siRNA-treated group ($n = 27$), untreated group ($n = 22$), control siRNA-treated group ($n = 4$), and buffer-treated group ($n = 8$). Since there was no significant difference in the results between the control siRNA-treated group and the buffer-treated group, we pooled the data together as a "mock-treated" group ($n = 12$). The results showed that the progressive body-weight loss of HD mice treated by siRNA-HDExon1 was slowed down compared with untreated and mock-treated groups (Fig. 2(A)). Mock-treated and untreated R6/2 transgenic mice start to lose body weight aggressively from around 8 to 9 weeks of age, while the loss was less severe in siRNA-HDExon1-treated R6/2 mice ($p < 0.01$ by ANOVA).

3.2.2. Longevity

The average longevity of HD mice received siRNA-HDExon1 treatment is 109.2 ± 12.3 (mean ± S.D., in days, $n = 39$), while it is 93.9 ± 9.2 days for mock-treated group ($n = 9$) and 95.7 ± 10.5 days for untreated group ($n = 65$). A comparative survival analysis (Kaplan–Meier method) clearly indicated that lifespan of siRNA-HDExon1-treated HD mice extended by more than 2 weeks (Fig. 2(B)). The effect was statistically significant ($p < 0.0001$ by log-rank test). Furthermore, among the 39 siRNA-treated R6/2 mice, three survived longer than 133 days, and one of these lived to 147 days (21 weeks). Therefore, treatment of siRNA-HDExon1 apparently slowed onset of HD-like phenotype and extended the life span of R6/2 mice.

3.2.3. Motor function

We assessed the effects of siRNA-HDExon1 on the motor function before and after HD-like symptoms onset. We first examined the feet-clasping phenotype which is commonly accepted as an indicator of HD-like disease onset in various HD mouse models (Menalled and Chesselet, 2002). Treatment with this siRNA clearly delayed the onset and reduced the frequency of the feet-clasping behavior triggered by tail suspension, which usually manifests at ~8 weeks of age for untreated R6/2 mice (Fig. 2(C and D), siRNA-treated, $n = 41$; mock-treated, $n = 12$; untreated, $n = 48$). This implied that siRNA treatments delayed the age of onset of HD symptoms by interfering with the expression of the transgenic mutant htt.

Rotarod tests were performed on R6/2 mice weekly at 6–8 weeks of age. siRNA-HDExon1-treated R6/2 mice ($n = 17$) performed significantly better than untreated R6/2 mice ($n = 11$; $p < 0.05$ by t-test; Fig. 3(A)) and were comparable to wild-type controls, thus indicating a beneficial effect of siRNA-treatment even at this stage. We also examined the pattern of free movement of mice at 9, 12 and 14 weeks of age using open-field equipment (Fig. 3(B)). siRNA-HDExon1-treated mice were more active than untreated or mock-treated R6/2 mice, especially at ages over 12 weeks. These data again suggest that siRNA-HDExon1 treatment can delay disease progression by about 2 weeks.

3.3. Pathological examinations

The formation of the intranuclear aggregation of mutant htt have been identified in human HD patients, and are accepted as pathological indicators of neuronal degeneration caused by mutated htt (DiFiglia et al., 1997). This NII formation is also a common phenomenon in both cell culture

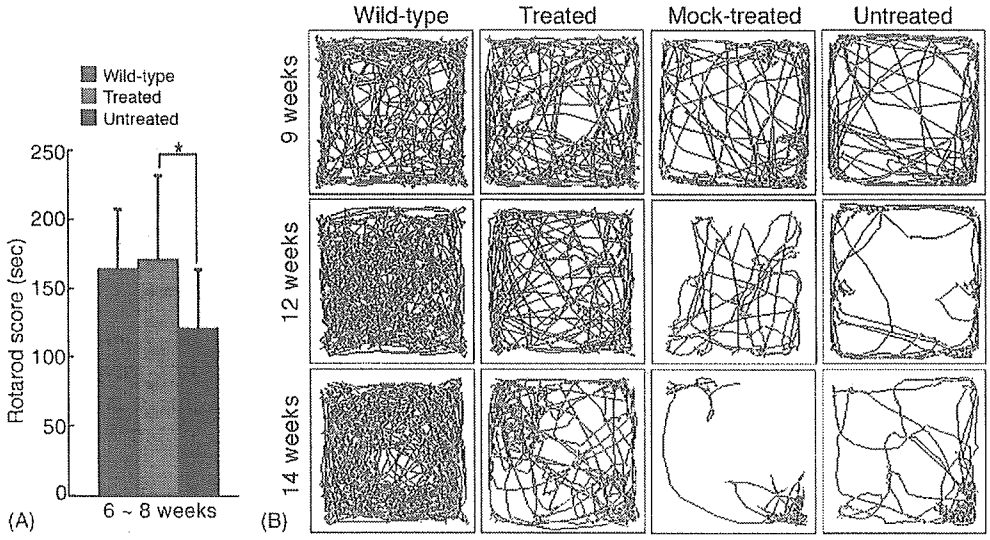

Fig. 3. Motor function assessment using a rotarod and open-field equipment. (A) R6/2 mice treated with siRNA-HDExon1 showed significant improvement on the rotarod at 6–8 weeks of age (t-test, $^{*}p < 0.05$; siRNA-treated, $n = 17$; mock-treated, $n = 10$; untreated, $n = 11$). (B) Open-field test. Trace comparison for age-matched groups of wild-type, siRNA-HDExon1-treated, mock-treated, or untreated R6/2 mice. siRNA-HDExon1-treated mice were more active than untreated or mock-treated R6/2 mice, especially at ages over 12 weeks.

models and in model animals. In HD transgenic mice, NII formation is commonly accepted as a pathological hallmark (Menalled and Chesselet, 2002). Because the transcription level relates to protein expression, the relative amounts of htt mRNA were estimated by real-time PCR to investigate the duration of the effect of siRNA on htt mRNA levels. The results showed that the suppression of htt mRNA was maintained for more than 1 week (Fig. 4(A)). The amount of htt aggregates in the striatum, as estimated by Western blotting, was reduced in the nuclear fraction of siRNA-treated mice (Fig. 4(B)). The soluble htt was not detected as previously reported (Tanaka et al., 2004). Therefore, siRNAs against transgenic htt induced the degradation of htt mRNA, which in turn resulted in a reduction of intranuclear aggregations on mutant htt. This confirms that siRNA treatment is pathologically beneficial.

The ventricles of untreated R6/2 mice (>8 weeks of age) were larger than those of wild-type mice, due largely to general brain atrophy and compensation by the ventricular system. SiRNA-HDExon1 treatment lessened the severity of this defect (Fig. 5(A)). As mentioned above, the occurrence of NII in brain neurons are widely accepted as pathological indicators of neuronal degeneration caused by mutated htt containing a poly Q in the R6/2 mouse model. In our experiments, immunohistochemical analysis of mouse brains using an antibody against htt clearly demonstrated that siRNA treatment reduced the prevalence of aggregates in the striatum compared with untreated or mock-treated R6/

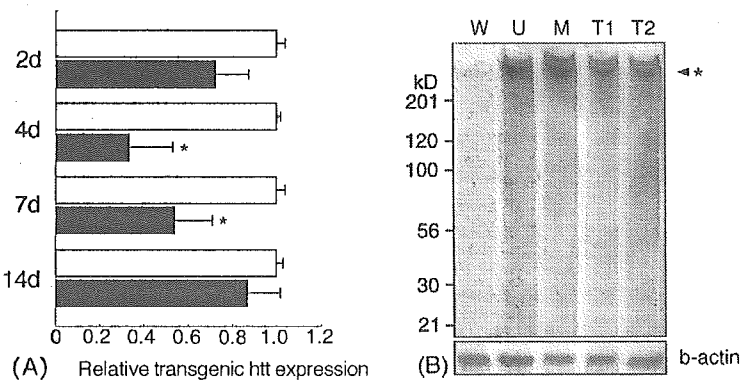

Fig. 4. siRNA-HDExon1 significantly reduces huntingtin transgenic mRNA and protein levels in brain tissues of R6/2 mice. (A) RNA from whole brain extracts was isolated, and huntingtin transgenic mRNA was determined by real-time PCR. siRNA-HDExon1-treated mice (black bars) suppressed transgene mRNA compared with the control group (combined mock-treated and untreated mice, white bars). Transgene expression was maximally repressed at 4 days post-transfection in vivo, and its effects lasted for at least 7 days ($n = 3$ for each group, $^{*}p < 0.01$). (B) Western blots of huntingtin aggregates in striatal tissue (50 μg per lane, nuclear extracts) from each group at 8 weeks of age. W, wild-type; U, untreated; M, mock-treated; T1, siRNA-treated mouse #1; T2, siRNA-treated mouse #2. Aggregated proteins remained in the gradient gel, as indicated (*, >200 kDa).